The glycolysis/HIF-1α axis defines the inflammatory role of IL-4-primed 2 macrophages

Shih-Chin Cheng (✉ jamescheng@xmu.edu.cn)
Xiamen University https://orcid.org/0000-0003-1251-8774

Buyun Dang
Xiamen University

Jia Zhang
Xiamen University

Qingxiang Gao
Xiamen University

Qiumei Zhong
Xiamen University

Lishan Zhang
Xiamen University

Yanhui Zhu
Xiamen University

Junqiao Liu
Xiamen University

Yujia Niu
Xiamen University

Nengming Xiao
Xiamen University https://orcid.org/0000-0001-5417-707X

Wen-Hsien Liu
School of Life Sciences, Xiamen University https://orcid.org/0000-0003-2500-3892

Kairui Mao
xiaman University, China https://orcid.org/0000-0003-2321-870X

Shu-hai Lin
Xiamen University https://orcid.org/0000-0002-4782-5320

Jialiang Huang
Xiamen University

Stanley Huang
Case Western Reserve University https://orcid.org/0000-0002-6557-3737

Ping-Chih Ho
University of Lausanne https://orcid.org/0000-0003-3078-3774

Article

Keywords: IL-4, M2 macrophage, Hif-1, glycolysis, epigenetic

Posted Date: November 16th, 2022

DOI: https://doi.org/10.21203/rs.3.rs-1322480/v2

Additional Declarations: (Not answered)

Title: The glycolysis/HIF-1α axis defines the inflammatory role of IL-4-primed macrophages

Authors:

Buyun Dang[1,2,6], Qingxiang Gao[1,6], Lishan Zhang[1,6], Jia Zhang[1,6], Hanyi Cai[1,6], Yanhui Zhu[1], Qiumei Zhong[1], Junqiao Liu[1], Yujia Niu[1], Kairui Mao[1], Nengming Xiao[1], Wen-Hsien Liu[1], Shu-hai Lin[1], Jialiang Huang[1], Stanley Ching-Cheng Huang[3], Ping-Chih Ho[4,5], Shih-Chin Cheng[1,2,7]

Affiliations:

[1]State Key Laboratory of Cellular Stress Biology, School of Life Science, Faculty of Medicine and Life Sciences, Xiamen University, Xiamen 361102, China

[2]Department of Gastroenterology, Zhongshan Hospital, School of Medicine, Xiamen University, Xiamen, Fujian, China

[3]Department of Pathology, Case Western Reserve University School of Medicine, Cleveland, OH, USA

[4]Ludwig Institute for Cancer Research, University of Lausanne, Epalinges, Vaud, Switzerland

[5]Department of Oncology, University of Lausanne, Epalinges, Switzerland

[6]These authors contributed equally to this work

[7]Correspondence: jamescheng@xmu.edu.cn

Keywords: IL-4, M2 macrophage, Hif-1α, glycolysis, epigenetics

Summary

T helper type 2 (Th2) cytokine-activated M2 macrophages play a major role in inflammation resolution and wound healing. Myriads of studies have demonstrated the anti-inflammatory feature of M2 macrophages. In the present study, we report that IL-4-primed macrophages respond more robustly to the subsequent LPS stimulation despite maintaining the canonical M2 signature gene expression. The canonical M2 and non-canonical proinflammatory-prone macrophages ($M2_{INF}$) diverge metabolically after the common IL-4Ra/Stat6 axis. While the Gln/α-KG/Jmjd3 axis is indispensable for M2 differentiation, the glycolysis/Hif-1α axis is critical for IL-4-induced $M2_{INF}$. The elevated glycolysis sustains Hif-1α stabilization and the pro-inflammatory phenotype of $M2_{INF}$. Conversely, inhibition of glycolysis blunts Hif-1α accumulation and $M2_{INF}$. Macrophages from myeloid-specific *Hif-1α* KO mice retain M2 differentiation capacity but fail to induce $M2_{INF}$. Wdr5-dependent H3K4me3 epigenetic modification mediates the long-lasting effect of IL-4 as the knocking down of *Wdr5* inhibits $M2_{INF}$. Moreover, the induction of $M2_{INF}$ by IL-4 intraperitoneal injection and transferring of $M2_{INF}$ provides a survival advantage against bacterial infection *in vivo*. To conclude, our findings delineate the previously neglected non-canonical role of $M2_{INF}$. This will broaden our understanding of IL-4-mediated physiological changes and provide immediate impacts on how Th2-skewed infections could re-direct disease progression in response to pathogen infection.

Main Text:

IL-4 is a prototypic immunomodulatory cytokine with diverse functions, such as regulation of immunoglobulin isotype switch(Fujieda et al., 1995; Lebman and Coffman, 1988), induction of MHC II(Stuart et al., 1988) and CD23 expression(Sarfati et al., 1990), regulation of hematopoiesis(Sonoda, 1994), etc. Amongst its multiple functions, the canonical role of IL-4 is to induce alternative macrophage activation, also known as M2(Locati et al., 2020; Orecchioni et al., 2019). M2 macrophages are traditionally regarded as anti-inflammatory macrophages, secreting Arginase-1, IL-10, TGF-β, and other anti-inflammatory cytokines, promoting the resolution of inflammation, wound healing and favoring tumor development and progression in the context of tumor-associated macrophages (TAMs). Upon binding to IL-4Rα, IL-4 induces the phosphorylation of STAT6, which dimerizes and translocates into the nucleus to promote the transcription of M2 signature genes.

Although M1/M2 polarization is a well-defined paradigm to explain the dichotomy of macrophage differentiation *in vitro*, macrophages in a pathophysiological or homeostatic state usually express mixed M1/M2 signature markers *in vivo*(Orecchioni et al., 2019; Sica and Mantovani, 2012). Therefore, a revised view concerning macrophage activation or differentiation will be a spectrum or continuum concept, highlighting the plasticity nature of macrophage activation/differentiation. For example, macrophages encountering invaded pathogens would be readily activated via the recognition of PRRs (Pattern recognition receptors)-PAMPs (Pathogen-associated molecular patterns), differentiated into proinflammatory M1-like macrophages during the acute inflammatory phase. However, the inflammatory response must be resolved when the host immune system clears up the invaders. Therefore, the proinflammatory M1 switch towards anti-inflammatory M2 macrophages over time to dampen inflammation and execute wound healing at the resolution phase.

Repolarization of macrophage phenotype is considered a potential therapeutic intervention approach in different diseases or pathological settings. For example, shifting pro-tumor TAM from M2 towards M1 phenotype might be beneficial in fighting cancer(Genard et al., 2017). Reprogramming proinflammatory M1 towards M2 might be favorable in ameliorating proinflammatory diseases such as obesity(Kammoun, 2014) and atherosclerosis(Bäck et al., 2019). We unexpectedly found that despite being IL-4-primed, macrophages expressing typical M2 signature genes such as *Arg1* and *Retnla* at basal state possess robust proinflammatory potential

upon LPS stimulation than naïve and M1 macrophages. We speculate that the long-held view concerning IL-4-induced M2 macrophages is worthy of reconsideration, as this is only partially true in the context when M2 macrophages do not encounter subsequent proinflammatory stimuli, such as LPS or other PAMPs. Here, we uncover a non-canonical proinflammatory-prone feature of IL-4 and delineate that IL-4-induced canonical M2 and non-canonical $M2_{INF}$ diverge metabolically after the common IL-4Ra/Jak1/Stat6 axis, with elevated glycolysis/Hif-1α as the defining factor for IL-4 non-canonical $M2_{INF}$ arm and Gln/α-KG axis responsible for canonical M2 arm. We further demonstrate that IL-4 induces non-canonical $M2_{INF}$ *in vivo* and renders mice more resistant to bacterial infection. Therefore, we report this previously neglected non-canonical aspect of IL-4 biology in macrophages which might open up a new vista to broaden our understanding of the unresolved association between type 2 immunity-bias diseases, such as asthma and allergy, and other inflammatory diseases, such as sepsis(Zein et al., 2017) and obesity(Bantulà et al., 2021; Peters et al., 2018).

Results

IL-4 induces non-canonical proinflammatory $M2_{INF}$

Mouse bone marrow-derived macrophages (BMDMs) polarization and repolarization capacity were examined *in vitro* by stimulation with LPS/IFNγ or IL-4 (**Fig. S1A**). Surprisingly, M2 macrophages induced higher M1 gene expression (**Fig. S1B**) and secreted more TNF-α, IL-6, and nitric oxide (NO) upon LPS/IFNγ stimulation (**Fig. S1C**). However, per previous reports(Bailey et al., 2019), M1 macrophages failed to repolarize to M2, as evidenced by the expression of *Arg1* and *Retnla* (**Fig. S1D**). Therefore, we speculate that, on the one hand, the canonical function of IL-4 is to induce M2 macrophage differentiation. On the other hand, IL-4 induces a non-canonical effect to "inflame" $M2_{INF}$ macrophages upon subsequent stimulation. To examine the non-canonical role of IL-4, we pretreated BMDMs with IL-4 for 24 hours and rested for additional 24 hours in a fresh medium before subsequent LPS stimulation **(Fig. 1A)**. As a result, *Il6*, *Il1β*, and *Il12a* gene expression (**Fig. 1B**) and IL-6 and NO secretion as well as intracellular pro-IL-1β level were upregulated (**Fig. 1C and Fig. S1E)**). These results suggest that IL-4 treatment primes macrophages to be more proinflammatory upon subsequent stimulation. We next investigated whether the duration of IL-4 stimulation modulates macrophage phenotype **(Fig. 1D)**. Macrophages received persistent IL-4 signaling for 48h (p-$M2_{INF}$) produced higher IL-6 and NO than the 24h exposure group ($M2_{INF}$) (**Fig. 1E**), albeit maintaining the high expression of M2

signature genes *Retnla* and *Arg1* (**Fig. 1F**), suggesting a persistent IL-4 stimulation induces a heightened proinflammatory effect while maintaining M2 signature gene expression. Moreover, when IL-4-treated BMDMs were stimulated simultaneously with LPS and IL-4, the *Il6* expression was further boosted while *Il10* was dampened **(Fig. S1F)**

Intrigued by the fact that IL-4 induces a more robust proinflammatory response in macrophages upon stimulation, we wondered whether other type 2 cytokines have a similar effect. We found that IL-13, but not IL-5, upregulated proinflammatory phenotype in BMDMs (**Fig. 1G** and **Fig. S1G**), suggesting the signaling transduction via IL-4Rα might be crucial in the non-canonical function observed. Surprisingly, the type 1 cytokine IFNγ failed to induce proinflammatory phenotype. Instead, pretreatment of IFNγ induced higher *Il10* expression upon subsequent LPS stimulation **(Fig. S1H)**. Stimulation with IFNγ and IL-4 simultaneously induced a similar response as IL-4 single stimulation (**Fig. 1G and S1G**), suggesting the presence of IL-4 plays a dominant effect in mounting $M2_{INF}$. Together, these results imply that the non-canonical $M2_{INF}$ could be elicited after both acute and persistent IL-4 exposure in type 2 responses where IL-4 and IL-13 levels are upregulated.

IL-4 induces $M2_{INF}$ in a IL-4Ra/Stat6-dependent and Gln/α-KG/Jmjd3 axis-independent manner

IL-4Ra is the common receptor for IL-4 and IL-13 signaling. As expected, IL-4 failed to induce M2 polarization in BMDMs derived from IL-4Ra MKO (*IL-4Ra 1α f/f Lyz2-cre* Myeloid specific KO) **(Fig. S2A).** Furthermore, the induction of $M2_{INF}$ was also impaired in IL-4Ra MKO **(Fig. 2A)**. Stat6-phosphorylation downstream of IL-4Ra is critical for IL-4-induced M2 polarization. Knocking down of Stat6 by shRNA impaired IL-4 mediated M2 genes *Arg1* **(Fig. S2B)**. Meanwhile, IL-4-induced $M2_{INF}$ was also inhibited as *IL-6* and *IL-1β* expression was reduced **(Fig. 2B),** suggesting that Stat6 is indispensable for IL-4-induced canonical M2 and non-canonical $M2_{INF}$.

As Glutamine/α-ketoglutarate/Jmjd3 axis is critical for IL-4-induced M2 polarization(Liu et al., 2017; Satoh et al., 2010), we further investigated whether this axis is responsible for the non-canonical $M2_{INF}$. In line with the previous report, M2 signature genes such as *Arg1* and *Retnla* were downregulated in glutamine-free conditions (**Fig. 2C**), while the proinflammatory genes (**Fig. 2D**), protein and NO expression (**Fig. 2E**) were not influenced. Inhibition with glutaminolysis or Jmjd3 (Jumonji C domain containing 3) activity by BPTES or GSK-J4 also impaired M2

signature gene expression (**Fig. S2C&D**). However, treating BPTES and GSK-J4 inhibited proinflammatory response despite the absence of IL-4, thus preventing us from assessing their role in IL-4-induced non-canonical effect (**Fig. S2E&F**). To circumvent this caveat, IL-4-treated BMDMs were rested for additional 5 days before restimulation, and by that time, the acute inhibition effect of BPTES and GSK-J4 was washed away. Nevertheless, the non-canonical IL-4-induced proinflammatory cytokines remained unaffected by both inhibitors **(Fig. 2F&G)**. Together, these results suggest that IL4/Stat6 axis is indispensable for both canonical M2 and non-canonical $M2_{INF}$, while Gln/α-KG/jmjd3 axis is critical for M2 but not involved in $M2_{INF}$.

Transcriptomics analysis reveals the inflammatory-prone feature of $M2_{INF}$

We further performed RNA-seq analysis to acquire a panoramic view of the transcriptomic profile induced by IL-4. There were 610 differential expression genes between the control and IL-4-treated groups, including classic M2 genes *Retnla*, *Chil3* and *Mgl2* in the top regulated genes, shown in the volcano plot **(Fig. 3A)**. In line with previous report(He et al., 2021), oxidative phosphorylation was among the topmost enriched metabolic pathway in upregulated genes by KEGG analysis **(Fig. 3B)**. As metabolic reprogramming plays a pivotal role in macrophage activation, we performed the Gene Set Enrichment Assay (GSEA) analysis with special focus on the metabolic pathways to find out which functional phenotypes were enriched in IL-4 group and associated with its non-canonical feature. Pathways such as oxidative phosphorylation, glucose catabolic process, and specifically glycolysis were significantly enriched in IL-4-treated macrophages **(Fig 3C)**.

We further compared the gene expression profile focusing on LPS upregulated genes **(Fig. S3A)**. LPS upregulated classic pathways including TNF, Nf-κb and cytokine/chemokine signaling pathways **(Fig. S3B)**. We subdivided the differential expressed genes into 3 clusters: C1 (upregulated), C2 (unaffected), and C3 (downregulated) by comparing the expression level between control and IL-4-treated macrophages and the performed enriched KEGG pathways enrichment analysis in each cluster were analyzed by KEGG (**Fig. 3D and Fig. S3C).** Proinflammatory genes, such as *Il6*, *Il12a*, and *Il1β*, were encompassed in cluster C1 in line with the qPCR results (**Fig. 1B**). The GO enrichment analysis of the C1 also revealed the enrichment of TNF, Nf-κb and Toll-like receptor signaling pathways (**Fig. 3E**), supporting the idea that the non-canonical feature of IL-4 in promoting proinflammatory response.

$M2_{INF}$ is more energetic and switches toward glycolysis upon LPS stimulation

Metabolic rewiring from oxidative phosphorylation towards glycolysis is essential for mounting efficient proinflammatory responses in macrophages(Viola et al., 2019). As glycolysis is upregulated by IL-4 pretreatment from our RNAseq analysis **(Fig. 3C)**, we further examined the cellular metabolic profile of IL-4-treated macrophages. Lactate production significantly increased in IL-4-treated macrophages upon LPS stimulation (**Fig. 4A**). In line with the elevated lactate level, essential glycolysis proteins such as Hk3, Pfkfb3, enolase1, and main glucose transporter Glut1 also increased (**Fig. 4B**). These results indicate that the robust shift towards glycolysis metabolically underlines the elevated proinflammatory feature of $M2_{INF}$.

We further assess the effect of IL-4 on the energetic status of macrophages. In line with the increased lactate secretion, IL-4-treated macrophages upregulated glycolysis both at basal and upon LPS stimulation and have a higher glycolytic capacity (**Fig. 4C**). Basal respiration, ATP production, and maximal respiration capacity are also increased by acute IL-4 treatment (**Fig. 4D**). Overall, IL-4 treated macrophages are more energetic at the basal and upon stimulation (**Fig. 4E**).

We further performed stable isotope tracing in IL-4 stimulated macrophages with the tracer [U-$^{13}C_6$]-Glucose. In agreement with the Seahorse results (**Fig. 4C**), ^{13}C-labeled glycolytic intermediates were significantly increased in IL-4 stimulated macrophages (**Fig. 4F**). Furthermore, the proportion of ^{13}C-labeled TCA cycle intermediates, such as citrate, α-ketoglutarate, succinate, and fumarate, was also primarily upregulated in IL-4 stimulated macrophages (**Fig. S4**), implying higher oxidative phosphorylation (OXPHOS) capacity which is in line with the oxygen consumption rate (OCR) result (**Fig. 4D**). Together, our metabolic analysis reveals that IL-4 treated macrophages, on the one hand, have upregulated OXPHOS capacity which is the metabolic feature of M2 macrophages. On the other hand, the elevated glycolysis at both basal and activation states might be critical for the proinflammatory $M2_{INF}$.

Glycolysis-mediated Hif-1α stabilization is critical for $M2_{INF}$

Hif-1α stabilization was shown to sustain prolonged IL-1β expression through succinate accumulation(Tannahill et al., 2013). We therefore assess the role of glycolysis/Hif-1α axis by glycolytic inhibitor 2-deoxyglucose (2-DG) in IL-4-treated macrophages. The accumulation of Hif-1α and upregulation of pro-IL-1β and IL-6 were inhibited by 2-DG **(Fig. 5A&B)**. Similarly, the heightened Hif-1α accumulation and pro-IL-1β and IL-6 level were blocked when IL-4-treated macrophages were cultured in a glucose-free medium **(Fig. 5C&D)** or galactose-replacing medium **(Fig. 5E&F)**. Since the intracellular succinate level was upregulated in IL-4-treated macrophages

(Fig. 5G), we further examined the causal relationship between upregulated glycolysis and accumulated succinate level by blocking with a mitochondrial pyruvate carrier inhibitor UK5099. The Hif-1α and pro-IL-1β level were also impaired by UK5099 **(Fig. 5H&I)**, suggesting mitochondrial pyruvate influx is crucial for the proinflammatory phenotype for $M2_{INF}$.

We further assessed whether Hif-1α is also involved in IL-4-induced M2 differentiation in myeloid-specific *Hif-1α* MKO BMDMs (*Hif-1α f/f Lyz2-cre* Myeloid specific KO). Our results suggested that IL-4-induced M2 genes *Arg1* and *Retnla* expression were not influenced in *Hif-1α* MKO BMDMs **(Fig. 5J)**, while IL-4-induced non-canonical augmentation of *IL-1β* expression was impaired **(Fig. 5K)**. These results suggest the glycolysis/Hif-1α axis is critical for IL-4-induced $M2_{INF}$.

Epigenetic determination of $M2_{INF}$

Metabolic rewiring and epigenetic modification have been closely associated with macrophage differentiation status. Therefore, we performed ATAC-seq to compare the chromatin accessibility of genes regulated by IL-4 in BMDMs. The promoter region (<1 Kb) has more enriched peaks in IL-4-treated BMDMs, suggesting IL-4 effect most likely takes place in the promoter region **(Fig. 6A)**. As expected, M2 signature genes *Arg1*, *Ccl22* and *Egr2* had more accessible chromatin regions, and higher gene expression in IL-4 stimulated macrophages (**Fig. 6B**). To gain a global view about the change of the epigenetic landscape, we performed GSEA analysis by concatenating the enriched peaks within 1Kb of the promoter region. In accordance with RNAseq results, oxidative phosphorylation, fatty acid oxidation and retinol metabolism were enriched in IL-4 treated BMDMs **(Fig. 6C & Fig. S5A)**. Both glycolysis and cytokine pathways were enriched in IL-4 treated BMDMs, reinforcing the epigenetic phenotype of $M2_{INF}$ **(Fig. 6D)**. As H3K4me3 is the epigenetic marker enriched at the active promoter region, we further performed an H3K4me3 Cut&Tag to visualize the active promoter. We found that most glycolysis genes such as *Hk3, Pfkfb3* and *Slc1a2 (Glut1)* **(Fig. 6E))** were also enriched with H3K4me3 peaks. Noteworthily, ATAC peaks were also enriched in the promoter region of proinflammatory genes such as *Il6, Il1β,* and *IL12b,* but no difference in the H3K4me3 peaks **(Fig. S5B)**, suggesting IL-4 treatment opens up the chromatin structure of proinflammatory genes while no active transcription activity at basal state.

As H3K4me3 has previously been reported to be the epigenetic landmark of β-glucan-induced trained immunity in macrophages, we further examined whether histone methylation is involved

in IL-4-induced non-canonical $M2_{INF}$. There were no obvious transcriptional regulation of writers and erasers of H3K4me3 in the IL-4-treated macrophages as revealed by RNAseq **(Fig. S5C)**. As Wdr5 forms a complex with Mll and Set H3K4 histone methyltransferase family, we knocked down Wdr5 and found that IL-4-induced augmentation of *Il6* and *Il1β* expression was partially inhibited (**Fig. 6F** and **Fig. S5D**), suggesting a potential role of H3K4 methylation in $M2_{INF}$. Furthermore, inhibition of histone methylation by MTA (pan-methyltransferase inhibitor) impaired IL-4 induced *IL-6* and *IL-1β* gene expression (**Fig. 6G**) and the production of IL-6 and NO (**Fig. S5E**), while MTA did not influence IL-4 induced M2 differentiation (**Fig. S5F**). Putting together the data from the glutamine deficiency experiment, we speculate that IL-4, on the one hand, could induce canonical M2 gene expression via the Gln/α-/Jmjd3 axis(Liu et al., 2017; Satoh et al., 2010). On the other hand, IL-4 might induce $M2_{INF}$ via Wdr5/H3K4me3 axis with persistent epigenetic memory to bolster glycolysis/Hif-1α upon LPS stimulation.

IL-4 induced $M2_{INF}$ *in vivo*

IL-4c has been reported to induce strong M2 macrophage differentiation *in vivo*(Huang et al., 2016). Therefore, to assess whether IL-4c treatment also induces $M2_{INF}$ *in vivo*, LPS were injected into the peritoneal cavity one-day post-IL-4c injection. IL-6 and TNF-α levels were significantly enhanced in serum (**Fig. 7A**) and peritoneal fluid (**Fig. S6A**) upon LPS stimulation. In addition, IL-4 pretreated mice were more susceptible to LPS-induced sepsis **(Fig. 7B)**, presumably due to the increased cytokine storm induced by IL-4. We further performed qPCR in purified peritoneal macrophages and found that basal expression of M2 genes *Arg1* and *Retnla* were significantly increased in IL-4c pretreated mice **(Fig. 7C)**. However, they still produced more proinflammatory cytokines upon LPS stimulation **(Fig. 7D)**. These results suggest that IL-4 executes both canonical M2 and non-canonical $M2_{INF}$ *in vivo*.

Since proinflammatory M1 macrophages have the strong bactericidal capacity, we wondered whether $M2_{INF}$ also possesses enhanced bactericidal ability *in vivo*. We found that IL-4c pretreated mice were more resistant to *Staphylococcus aureus* infection (**Fig. 7E**), suggesting IL-4c pretreatment renders host survival advantage against bactericidal infection. As IL-4 has been reported to modulate myelopoiesis(Snoeck et al., 1993), we further delineated the IL-4c-induced protection is due to the induction of $M2_{INF}$ or increase of myelopoiesis. We found the acute treatment of IL-4c did not influence both total cell numbers of circulating and peritoneal $Ly6C^{hi}$ monocytes and eosinophils, while $Ly6G^{+}$ neutrophils decreased in number, albeit not significant

(Fig. S6B). The drop of neutrophils is in line with the report that IL-4 antagonizes bone marrow egression of neutrophils(Woytschak et al., 2016).

We further explored the potential role of $M2_{INF}$ in an OVA-induced allergy model. Compared to control mice, OVA-primed mice were more resistant to *S. aureus* infection (**Fig. 7F**). Furthermore, the bacterial blood CFU is significantly lower in the OVA-primed group, suggesting that acute allergy response induced an enhanced bactericidal effect in mice **(Fig. S6C)**. We further confirmed that *Arg1* and *Rentla* were explicitly upregulated in peritoneal macrophages isolated from the OVA-treated group (**Fig. S6D**), confirming the triggering of type 2 response *in vivo*. Moreover, when peritoneal macrophages were stimulated with LPS *ex vivo*, macrophages isolated from the OVA group induced more robust proinflammatory genes (**Fig. 7G**). As type 2 immunity induced eosinophilia and ILC2 were shown to play roles in protection against bacterial infection(Krishack et al., 2019), we further examined the role of $M2_{INF}$ in OVA-induced allergy model in the *IL-4Ra* MKO (*IL-4Ra f/f Lyz2-cre*). Our results demonstrated that *IL-4Ra* MKO mice were not protected in the OVA-allergy model, highlighting that IL-4Ra is essential in induction of $M2_{INF}$ **(Fig. 7H)**. Our data suggest that type 2 immune response induces $M2_{INF}$, producing more proinflammatory cytokines and more resistance to bacterial infection in animal models.

Discussion

The canonical role of IL-4 in inducing M2 macrophage differentiation and mediating anti-inflammatory responses is well documented. Furthermore, the signaling transduction and pathway involved in IL-4-induced M2 differentiation are well characterized. However, an unrecognized proinflammatory-prone non-canonical feature of IL-4 was left unnoticed. We report that pre-conditioning with IL-4 induces a non-canonical $M2_{INF}$ with a robust proinflammatory potential upon microbial stimulation.

Metabolic rewiring and epigenetic control have been reported to play critical roles in canonical M2 macrophage polarization. Jha et al. demonstrated that M2 polarization activates glutamine catabolism and UDP-GlcNAc-associated modules(Jha et al., 2015). When macrophages were polarized towards M2 in glutamine deprived medium or with N-glycosylation inhibitor tunicamycin, M2 polarization and production of Ccl22 were significantly reduced. In addition, Jmjd3, an H3K27me3 demethylase, has been upregulated by IL-4 during M2 polarization, and knockdown of *Jmjd3* also impairs M2 polarization *in vitro*(Ishii et al., 2009). Furthermore, helminth-induced M2 polarization is significantly reduced in *Jmjd3*$^{-/-}$ mice(Satoh et al., 2010). α-

ketoglutarate has recently been demonstrated as a central hub bridging glutamine metabolism and Jmjd3-mediated epigenetic programming in M2 macrophages(Liu et al., 2017). In addition to glutaminolysis, α-ketoglutarate is also derived as a by-product of the de novo serine synthesis pathway via the upregulation of phosphoglycerate dehydrogenase (Phgdh) activity induced by IL-4(Wilson et al., 2020). Although the Gln/α-KG/Jmjd3 axis has been demonstrated to be crucial for IL-4 mediated M2 differentiation via downregulating H3K27me3, this axis is dispensable for the non-canonical proinflammatory feature induced by IL-4 in macrophages. Our data suggest that IL-4 treatment, on the one hand, induces M2 gene expression via Stat6- and Gln/α-KG/Jmjd3-axis, which opens up the promoter region of M2 signature genes by downregulation of the H3K27me3(Liu et al., 2017; Satoh et al., 2010). On the other hand, IL-4 induces $M2_{INF}$ with a robust proinflammatory feature via recruiting Wdr5 interacting H3K4 methyltransferase, upregulating H3K4me3 around the promoter region of the glycolysis genes, supporting the enhanced glycolysis feature of $M2_{INF}$. The H3K4me3 marked promoters serve as epigenetic memory, facilitating a higher transcription activity upon stimulation resulting in a more robust glycolytic switch, Hif-1α stabilization and subsequent proinflammatory phenotype. Metabolically, IL-4 stimulated macrophages are more energetic with higher basal respiration rate and elevated glycolysis at basal while switching toward robust glycolysis upon stimulation and having higher glycolytic capacity. Inhibition of glycolysis and mitochondrial pyruvate carrier impairs Hif-1α accumulation and subsequent upregulation of proinflammatory cytokine expression. Metabolomics data reveal that IL-4 treated macrophages had elevated one-carbon metabolism, TCA cycle, and glycolysis. The elevated one-carbon metabolism may provide SAM as a methyl donor for epigenetic modification. Succinate accumulation is involved in Hif-1α stabilization and enhanced IL-1β expression(Tannahill et al., 2013) and subsequent H3K4me3 accumulation(Keating et al., 2020). Fumarate accumulation is involved in β-glucan-induced H3K4me3 accumulation(Arts et al., 2016). Therefore, the elevated intermediate TCA cycle metabolite accumulation in IL-4 stimulated macrophages might impact IL-4 induced $M2_{INF}$ via epigenetic modification. Moreover, Hif-1α stabilization is indispensable only for the non-canonical arm of IL-4 but does not influence canonical M2 differentiation.

It was reported that asthmatic patients had a decreased risk for hospital mortality, septicemia, sepsis, and septic shock across all infections(Zein et al., 2017). In a retrospective study, patients who survive *S. aureus* bacteremia have higher numbers of Th2 and fewer Th17 lymphocytes in the blood(Krishack et al., 2019), suggesting that type 2 immune response might have a beneficial

bactericidal effect in humans. In mice, a nematode infection has improved survival from septic bacterial peritonitis(Sutherland et al., 2011). Although the accumulation of mast cells and eosinophils has been suggested to play a role in the bactericidal effect in the acute type 2 immune response, the role of macrophages is mostly unrecognized in this scenario. Acute IL-4c injection has been demonstrated to induce peritoneal macrophage differentiation toward an M2-biased phenotype(Jenkins et al., 2013). However, *ex vivo* stimulation of peritoneal macrophages with IL-4 enhanced IL-6 and TNF-α production upon nematode *Neisseria meningitidis* infection(Varin et al., 2010) which is in accordance with the non-canonical $M2_{INF}$ phenotype described here. In addition to IL-4, another type 2 cytokine IL-13, but not IL-5, could also induce $M2_{INF}$ *in vitro*. Moreover, persistent IL-4 stimulation further boosts the proinflammatory response of $M2_{INF}$. Therefore, we wonder whether type 2 response could have an acute and chronic effect on macrophages *in vivo*. Mice injected with IL-4c were more susceptible to LPS-induced sepsis and secreted more IL-6 and TNF-α, suggesting acute IL-4 priming could enhance the proinflammatory response *in vivo*. This result is in line with a previous report demonstrating that pretreatment with peritoneal macrophage with IL-4 augments the production of cytokines and chemokines(Major et al., 2002). Moreover, IL-4 pretreatment mice were more resistant to *S. aureus* infection. In addition, the type 2 immune response induced by OVA also renders mice better protection against subsequent bacterial infection. The peritoneal macrophages from OVA-challenged mice have upregulated IL-6 production compared to control mice, suggesting that macrophages could acquire a proinflammatory phenotype in the acute type 2 immune response. Therefore, our data suggest an acute type 2 immune response could induce $M2_{INF}$ *in vivo*.

In contrast to our finding, Czimmerer et al. reported that IL-4 stimulated macrophages suppressed NLRP3 inflammasome activation and IL-1β secretion upon LPS stimulation in a STAT6-dependent manner(Czimmerer et al., 2018). This seemingly contradictory result could be due, at least partly, to the way of BMDMs differentiation. Czimmerer et al. used a conditioned medium from L929 cells, while we used recombinant M-CSF for BMDM differentiation. As L929 conditioned medium contains M-CSF and other soluble factors, such as macrophage migration inhibitory factor (MIF), osteopontin, Ccl2, and Ccl7, derived from L929, L929 conditioned medium differentiated macrophages were functionally different from recombinant M-CSF derived macrophages(Heap et al., 2021). In addition, they used *Helgmosomoides polygyrus* infection model to induce a type 2 immune response in mice. However, instead of assessing the role of IL-4 on peritoneal macrophages by bacterial infection, they examined the peritoneal macrophages

isolated from *H. polygyrus* infected mice *ex vivo* and showed that peritoneal macrophages from *H. polygyrus* infected group have lower *Nlrp3* and *Il-1b* expression upon LPS stimulation. In contrast, we adopted a different model to assess whether a prior type 2 response could induce the non-canonical effect of IL-4 *in vivo,* and the collective results point to the same effect that type 2 response causes a more robust proinflammatory response *in vivo* and renders a better protection capacity upon bacterial infection. In line with our report, Czimmerer et al. recently also reported that IL-4 priming induces extended synergy upon LPS stimulation via IL-4-directed remodeling, which is also observed in alveolar macrophages in the murine allergic inflammation model {Czimmerer:2022jn}. Interestingly, Lundahl et al. demonstrated that IL-4/IL-13 induced protective trained immunity against mycobacterial infection in macrophages via enhancing OXPHOS activity {Lundahl:2022iv}. Together, these recent reports together with our current finding reveals the biological significance of non-canonical $M2_{INF}$.

Although our current data showcase that Wdr5/H3K4me3-mediated epigenetic modification in the glycolysis genes supports the elevated glycolysis/Hif-1α-axis in $M2_{INF}$, there are still questions left to be answered. First, which specific H3K4me3 writer or eraser is directly responsible for the observed H3K4me3 modification? As the known H3K4me3 modifiers did not show significant change at transcriptional level via RNAseq analysis, it is very likely that the target H3K4me3 modifier is regulated post-translationally via the metabolites change induced by IL-4. Second, which chromatin modifier opens up the promoter region of proinflammatory genes? As these regions are enriched with ATAC peaks but not H3K4me3 peaks, different sets of modifiers seem to be involved in glycolysis genes and proinflammatory genes. Third, how long is the duration of the phenotype of $M2_{INF}$? We have shown that both acute and chronic exposure to IL-4 induced the $M2_{INF}$ in macrophages *in vitro*, it will therefore important to assess the duration of the $M2_{INF}$ *in vivo* as the inflammatory-prone consequence might impacts the type 2 immune-mediated diseases.

To sum up, we propose that IL-4 induced both canonical M2 and non-canonical $M2_{INF}$ via different epigenetic modifications. The non-canonical trained immunity induced by IL-4 is characterized by Wdr5/H3K4me3 axis, enabling the trained macrophages to be reprogrammed towards elevated glycolysis, leading to Hif-1α stabilization and subsequent more robust proinflammatory phenotype. Due to the association between asthma and chronic inflammatory diseases, such as obesity, or asthma and acute inflammatory response, such as sepsis, we believe a further

characterization of IL-4-induced $M2_{INF}$ will fill the gap between the Th2-biased disease asthma and chronic and acute inflammatory diseases. Thus, our data here provide a new vista considering the well-characterized anti-inflammatory cytokine IL-4 and offer a new horizon to cope with Th2 disease-associated inflammatory diseases.

Materials and Methods

Reagents

Recombinant M-CSF (CB34), IL-4 (CK74), IL-5 (CW73), IL-13 (CX57), and IFNγ (CM41) were purchased from Novoprotein, Shanghai, China. E. coli LPS (S11060), NT157 (S80314) were purchased from Shyuanye, Shanghai, China. BPTES, GSK-J4 (HY-15648B), Histone methyltransferase inhibitor MTA (HY-16938), UK5099(HY-15475) were purchased from MedChemExpress. 2-deoxy glucose (D8375), glucose (G7021), N-(1-Naphthyl) ethylenediamine dihydrochloride (N9125) and Sulfanilamide (S9251) were purchased from Sigma-Aldrich. SYBR Green Premix Pro Taq HS qPCR Kit (AG11701), Evo M-MLV reverse transcriptase (AG11605), recombinant RNase inhibitor (AG11608) were purchased from Accurate biology. Amplex Red (119171-73-2) was purchased from Alfachem.

Bone-Marrow-Derived Macrophage Culture and Differentiation

Bone marrow cells were harvested from femurs and tibia of 6–8-week-old C56BL6/J mice and differentiated in DMEM supplemented with 10 % FBS and 40 ng/ml of recombinant mouse M-CSF. Half volume of medium containing fresh 40 ng/ml of M-CSF was added to the cell culture at day 3. Differentiated BMDMs were detached, counted, and reseeded to the cell culture plate for subsequent experiments.

For macrophage polarization experiments, 20 ng/ml LPS and 100 ng/ml IFNγ were added to BMDMs to induce M1 macrophage polarization. 20 ng/ml IL-4 were used to induce M2 polarization. To assess the short-term effect of type 2 cytokines, BMDMs were cultured with 20 ng/ml of IL-4, IL-5, or IL-13. After 24 hours, BMDMs were washed with PBS once and stimulated with 100 ng/ml LPS to assess the cytokine production capacity. To assess IL-4 induced long-termed effect, BMDMs were first cultured with 20 ng/ml IL-4 for 24 hours and then washed with PBS once and refreshed with DMEM for additional 5 days. BMDMs were then harvested for subsequent functional assessment. To assess the signaling pathways involved in IL-4 induced canonical and noncanonical effects, BMDMs were pre-incubated with various inhibitors for 30

min prior IL-4 stimulation. BMDMs were washed with PBS 24 hours post-IL-4 stimulation and harvested for subsequent functional assessment.

Quantitative Real-Time PCR

For quantitative RT-PCR, total mRNA was extracted with oligo-dT magnetic beads. In short, RNA was extracted by magnetic beads conjugated with Oligo-dT18. Isolated RNA was reverse transcribed into cDNA using dNTP (Beyotime, D7366)/oligodT mix, RNA transcriptase (Accurate Biology, AG11605), and RNase inhibitor (Accurate Biology, AG11608). qPCR was performed using the SYBR Green method (Accurate Biology, AG11701). Relative expression levels were calculated using the ΔCT method and normalized to the expression of the β2M housekeeping gene. The primer sequences we used are listed in Table S1.

ELISA and Lactate Measurement

Cytokine levels in culture supernatant or mice serum were determined by TNF-α (Invitrogen; 88-7324-88) and IL-6 (Invitrogen; 88-7064-88) ELISA kits following the instructions of the manufacturer. As for lactate measurements, the cellular supernatant was diluted by PBS. Then the diluent is mixed with the mixture containing Amplex Red, HRP, and lactate oxidase for 10 min. The fluorescence was detected at excitation wavelength at 528 nm and emission wavelength at 590 nm by fluorescence plate reader.

NO Measurement

The cellular supernatant was mixed with solution A (ethylenediamine dihydrochloride) and solution B (sulfanilamide) in a one-to-one ratio. Then the absorbance was measured at 540 nm.

Assay for Transposase-Accessible Chromatin with high-throughput sequencing (ATAC-seq)

ATAC-seq was carried out mainly according to TruePrep DNA Library Prep Kit V2 for Illumina (Vazyme, TD501) with minor modification. Briefly, we spun 30,000 cells at 500 g for 5 min. Cells were lysed for 10 min at 4 ℃ by using pre-cold lysis buffer (10 mM Tris-HCl, pH 7.4, 10 mM NaCl, 3 mM MgCl2 and 0.1% IGEPAL CA-630). Nuclei were harvested for transposition reaction. After tagmentation, DNA was purified using the Agencourt AMPure XP kit (Beckman Coulter, A63880). To reduce GC and size bias, we determined the final PCR cycles using qPCR to allow library amplification to be stopped before saturation. We performed initial amplifications for five cycles, after which we took an aliquot of the PCR reaction and added 10 μl of the PCR cocktail with SYBR Green at a final concentration of 0.3×. We ran this reaction for 25 cycles to

calculate the additional cycles required for the remaining 45 μL reaction. We amplified library fragments for 12-13 cycles. The libraries performed double size selection for 300-500 bp DNA fragments. Fragment distribution of libraries was assessed with Agilent 4200. The library preparations were sequenced on an Illumina Hiseq platform, and 150 bp paired-end reads were generated.

CUT&Tag library preparation

CUT&Tag library was performed according to the NovoNGS® CUT&Tag 3.0 kit (N259-YH01-01A, Novoprotein). 100,000 sorted cells were captured by Con A beads. Cells-beads complex were incubated with primary H3K4me3 antibody (Cell signal technology CST 9751) and secondary Rabbit IgG antibody (abcam ab171870) at RT. The unbound antibodies and cells-beads complex were washed with antibody buffer. Tn5-pA/G was added to the cell-beads complex for transposition reaction at 37 °C. The DNA fragments were extracted, purified by extracted beads.

RNA Isolation and Sequence

RNA from cells was isolated using RNAprep Pure Cell/Bacteria Kit (TIANGEN) per instruction of the manufacturer. RNA samples were quantified by Qubit and an Agilent Bioanalyzer for the RNA integrity assessment. All samples had an RNA integrity number (RIN) of about 10. Following the manufacturer's recommendations, sequencing libraries were generated using NEBNext® UltraTM RNA Library Prep Kit for Illumina® (NEB, USA), and index codes were added to attribute sequences to each sample. The clustering of the index-coded samples was performed on a cBot Cluster Generation System using TruSeq PE Cluster Kit v3-cBot-HS (Illumia) according to the manufacturer's instructions. After cluster generation, the library was sequenced on an Illumina Novaseq platform, and 150 bp paired-end reads were generated.

Metabolomics

Bone marrow-derived macrophages (2×10^6) were seed in a 6-well plate and treated as above. Especially for metabolites tracing experiment, DMEM was replaced with glucose-free medium supplemented with 12.5 mM U-[^{13}C]-glucose (Cambridge Isotope Laboratories) with or without 4 mM glutamine (Gibco). For metabolites extraction, cells were washed three times with pre-cold PBS. After completely aspirating the liquid, the plates were put on ice, 1 ml of extraction buffer (volume ratio 4:1 methanol/water) was added and scraped on ice. The lysate was transferred to a 2 ml tube and vortex for 30 seconds, followed by additional 10 min sonication in the ice bath, and

then immediately frozen in a liquid nitrogen tank. The mixtures were centrifuged at 13,000 rpm for 15 min at 4 ℃. Finally, supernatants were transferred to a new tube and lyophilized.

For metabolites analysis, the liquid chromatography with SCIEX Exion LC AD was prepared, and all chromatographic separations were performed with a Millipore ZIC-pHILIC column (5 μm, 2.1× 100 mm internal dimensions, PN: 1.50462.0001). Column was maintained at 40°C and the injection volume of all samples was 2 μL. The mobile phase A composed by 15 mM ammonium acetate and 3 ml/L Ammonium Hydroxide (> 28 %) in LC-MS grade water. The mobile phase B is composed by LC−MS grade 90 % (v/v) acetonitrile in HPLC water. The mobile phase runs at a flow rate of 0.2 mL/min. The column was eluted with the following gradient program: 95% B held for 2 min, increased to 45 % B in 13 min, held for 3 min, and the post time was set 4 min. The QTRAP mass spectrometer used a Turbo V ion source. The ion source was run in negative mode with a spray voltage of -4,500 V, Gas1 40 psi and Gas2 50 psi and Curtain gas 35 psi. Metabolites were measured using the multiple reactions monitoring mode (MRM). The relative amounts of metabolites were analyzed by MultiQuant Software Software (AB SCIEX).

Animal

Wild-type C57BL/6 mice were purchased from Xiamen University Laboratory Animal Center. *Hif-1α*$^{f/f}$, *IL-4Ra*$^{f/f}$ and *Lyz2-cre* mice were purchased from GermPharmatech. All mice were maintained under specific pathogen-free conditions at the Xiamen University Laboratory Animal Center. These mouse experiments were approved by the Institutional Animal Care and Use Committee. In addition, they were in strict accordance with good animal practice as defined by the Xiamen University Laboratory Animal Center.

IL4c administration and LPS induced sepsis

For the administration of IL-4 complex (IL-4c), 5 μg of recombinant mouse IL-4 was complexed to 25 μg of anti-mouse IL-4 antibody (BioXCell,11B11), diluted in 200 μl of PBS and administered intraperitoneally. 24 hr post-IL-4c administration, mice were injected with 20 mg/kg LPS to induce sepsis. Serum was harvested from the caudal tail 2 hr post-LPS injection. ELISA determined the IL-6 and TNF-α levels in serum according to the manufacturer's instructions. Mice survival after LPS injection was monitored for 6 days.

OVA-induced Allergy model

C57BL/6 mice were intraperitoneally injected with 100 μg OVA (Sigma, A5253) absorbed to 10 % Alum (Sigma, A6435) with the final volume ratio of OVA to Alum as 1:1 on days 0 and 14.

Mice were intraperitoneally injected with 0.1 mg OVA in 200 μl PBS from days 21 to 25. Mice were intraperitoneally injected with Staphylococcus aureus with the dose of 1×10^4 CFU / 200 μL PBS per mouse. On day 27, whole blood from the caudal tail was collected for calculating the CFU.

BMDM adoptive transfer model

BMDMs were treated with 20 ng/ml IL-4 for 24 hours. Mice were adoptive transferred with 0.75 million IL-4-primed or control BMDM cells via intravenous injection. Mice were then subsequently infected with 1×10^4 CFU *Staphylococcus aureus* via intravenous injection and monitored for survival.

Western Blot

Cells were lysed with RIPA buffer (1 mM Tris-HCl, 0.3 M NaCl, 0.01% SDS, 1.5% NP40, 120 mM deoxycholate, 1 M $MgCl_2$) containing protease inhibitors. Proteins were resolved by SDS-PAGE and transferred to PVDF membranes (Roche, # 3010040001). The membranes were blocked for 1 h in blocking buffer (5% BSA and 0.1% Tween 20 in TBS) at room temperature and then incubated with respective primary antibodies in 5% BSA containing TBST at 4°C overnight. Membrane was then washed and subjected to HRP-coupled secondary antibodies in TBST at room temperature for 1 hour. Antibody against β-Actin (21338), pfkfb3(49656) was purchased from SAB. Antibodies against HK1 (A10886), HK3 (A8428), Glut1 (A11727), Histone H3(A2348), Acetyl-Histone H3K27 (A7253), Hif1α(A11945) were purchased from ABclonal. Antibodies against Aldolase A (8086), Enolase-1 (3810), Stat6 (5397), Mono-Methyl-Histone H3K4 (5326S), Tri-Methyl-Histone H3 (Lys4) (9751) were purchased from CST.

RNA-seq data analysis

Paired-end sequence reads were aligned to mouse genome reference (mm10) with HISAT2 and option as defaults. These reads mapping to each gene were named raw-count through feature-count. FPKM of each gene is based on the length of the gene and its raw count. The DESeq2 was used for differential gene expression analysis. Differentially expressed genes were selected by fold change and significance relative based on two biological replications. The significant genes show fold change above 2 with pvalues below 0.05. ClusterProfiler (R) was used in pathway analysis and the resulting padj (pvalue adjusted using Benjamini and Hochberg's) cut off 0.05. All heatmap are created with ComplexHeatmap in R. RNAseq data have been deposited in the GEO database with accession number GSE184811.

CUT&Tag-seq and ATAC-seq data analysis

The paired end reads were aligned to mouse reference genome(mm10) by bowtie2 and option as defaults. Samtools was used for format changing. MACS2 was used for peak calling with option p-value 0.05 and model fold 5-50 and keep-dup all. The peaks were counted by bedtools and normalization through RPKM. The ChIPseeker was used to annotate the peaks. ClusterProfiler was used for all pathways analysis. The msigdb_v2022.1.Mm was used for GSEA analysis.

Statistics

Differences were analyzed using the two-tailed Student's t-test. Analyses were performed using Prism (GraphPad Software). Significant difference was label with star sign (p-value < 0.05). Date is shown as means ±SD.

Acknowledgments:

Funding:

National Natural Science Foundation of China grant 32161133020 and 32070904 (S-CC)

Fundamental Research Funds for the Central Universities 20720220003 (S-CC)

Start-up fund of Xiamen University (S-CC)

European Research Council Starting Grant 802773-MitoGuide (P-CH)

SNSF project grant 31003A_182470 (P-CH)

Cancer Research Institute (P-CH)

Cancer Research Institute CLIP Investigator Award (SC-CH)

VeloSano Pilot Award (SC-CH)

Comprehensive Cancer Center American Cancer Society Pilot Grants IRG-91-022-19, IRG-16-186-21(SC-CH)

Author contributions:

Conceptualization: S-CC

Methodology: BD, QG, LZ, JZ, QZ, YH, JL, S-CC

Investigation: BD, QG, LZ, SL, JZ, YH, SC-CH, P-CH, S-CC

Funding acquisition: S-CC

Supervision: S-CC

Writing – original draft: DB, JZ, S-CC

Writing – review & editing: DB, QG, SL, JZ, NX, W-HL, KM, SL, JH, SC-CH, P-CH, S-CC

Declaration of interests:

The authors declare that they have no competing interests.

References

Arts, R.J.W., Novakovic, B., Horst, ter, R., Carvalho, A., Bekkering, S., Lachmandas, E., Rodrigues, F., Silvestre, R., Cheng, S.-C., Wang, S.-Y., Habibi, E., Gonçalves, L.G., Mesquita, I., Cunha, C., van Laarhoven, A., van de Veerdonk, F.L., Williams, D.L., van der Meer, J.W.M., Logie, C., O'Neill, L.A., Dinarello, C.A., Riksen, N.P., van Crevel, R., Clish, C., Notebaart, R.A., Joosten, L.A.B., Stunnenberg, H.G., Xavier, R.J., Netea, M.G., 2016. Glutaminolysis and Fumarate Accumulation Integrate Immunometabolic and Epigenetic Programs in Trained Immunity. Cell Metabolism 24, 807–819. doi:10.1016/j.cmet.2016.10.008

Bailey, J.D., Diotallevi, M., Nicol, T., McNeill, E., Shaw, A., Chuaiphichai, S., Hale, A., Starr, A., Nandi, M., Stylianou, E., McShane, H., Davis, S., Fischer, R., Kessler, B.M., McCullagh, J., Channon, K.M., Crabtree, M.J., 2019. Nitric Oxide Modulates Metabolic Remodeling in Inflammatory Macrophages through TCA Cycle Regulation and Itaconate Accumulation. CellReports 28, 218–230.e7. doi:10.1016/j.celrep.2019.06.018

Bantulà, M., Roca-Ferrer, J., Arismendi, E., Picado, C., 2021. Asthma and Obesity: Two Diseases on the Rise and Bridged by Inflammation. J Clin Med 10, 169.

Bäck, M., Yurdagul, A., Jr, Tabas, I., Öörni, K., Kovanen, P.T., 2019. Inflammation and its resolution in atherosclerosis: mediators and therapeutic opportunities. Nat Rev Cardiol 16, 389–406.

Czimmerer, Z., Daniel, B., Horvath, A., Ruckerl, D., Nagy, G., Kiss, M., Peloquin, M., Budai, M.M., Cuaranta-Monroy, I., Simandi, Z., Steiner, L., Nagy, B., Jr, Poliska, S., Banko, C., Bacso, Z., Schulman, I.G., Sauer, S., Deleuze, J.-F., Allen, J.E., Benko, S., Nagy, L., 2018. The Transcription Factor STAT6 Mediates Direct Repression of Inflammatory Enhancers and Limits Activation of Alternatively Polarized Macrophages. Immunity 48, 75–90.e6. doi:10.1016/j.immuni.2017.12.010

Fujieda, S., Zhang, K., Saxon, A., 1995. IL-4 plus CD40 monoclonal antibody induces human B cells gamma subclass-specific isotype switch: switching to gamma 1, gamma 3, and gamma 4, but not gamma 2. J Immunol 155, 2318–2328.

Genard, G., Lucas, S., Michiels, C., 2017. Reprogramming of Tumor-Associated Macrophages with Anticancer Therapies: Radiotherapy versus Chemo- and Immunotherapies. Front Immunol 8, 828. doi:10.3389/fimmu.2017.00828

He, L., Jhong, J.-H., Chen, Q., Huang, K.-Y., Strittmatter, K., Kreuzer, J., DeRan, M., Wu, X., Lee, T.-Y., Slavov, N., Haas, W., Marneros, A.G., 2021. Global characterization of macrophage polarization mechanisms and identification of M2-type polarization inhibitors. CellReports 37, 109955. doi:10.1016/j.celrep.2021.109955

Heap, R.E., Marín-Rubio, J.L., Peltier, J., Heunis, T., Dannoura, A., Moore, A., Trost, M., 2021. Proteomics characterisation of the L929 cell supernatant and its role in BMDM differentiation. Life Sci Alliance 4. doi:10.26508/lsa.202000957

Huang, S.C.-C., Smith, A.M., Everts, B., Colonna, M., Pearce, E.L., Schilling, J.D., Pearce, E.J., 2016. Metabolic Reprogramming Mediated by the mTORC2-IRF4 Signaling Axis Is Essential for Macrophage Alternative Activation. Immunity 45, 817–830. doi:10.1016/j.immuni.2016.09.016

Ishii, M., Wen, H., Corsa, C.A.S., Liu, T., Coelho, A.L., Allen, R.M., Carson, W.F., Cavassani, K.A., Li, X., Lukacs, N.W., Hogaboam, C.M., Dou, Y., Kunkel, S.L., 2009. Epigenetic regulation of the alternatively activated macrophage phenotype. Blood 114, 3244–3254. doi:10.1182/blood-2009-04-217620

Jenkins, S.J., Ruckerl, D., Thomas, G.D., Hewitson, J.P., Duncan, S., Brombacher, F., Maizels, R.M., Hume, D.A., Allen, J.E., 2013. IL-4 directly signals tissue-resident macrophages to proliferate beyond homeostatic levels controlled by CSF-1. J Exp Med 210, 2477–2491. doi:10.1084/jem.20121999

Jha, A.K., Huang, S.C.-C., Sergushichev, A., Lampropoulou, V., Ivanova, Y., Loginicheva, E., Chmielewski, K., Stewart, K.M., Ashall, J., Everts, B., Pearce, E.J., Driggers, E.M., Artyomov, M.N., 2015. Network integration of parallel metabolic and transcriptional data reveals metabolic modules that regulate macrophage polarization. Immunity 42, 419–430. doi:10.1016/j.immuni.2015.02.005

Kammoun, H.L., 2014. Macrophage polarization in obesity and type 2 diabetes: weighing down our understanding of macrophage function? Front Immunol 1–6. doi:10.3389/fimmu.2014.00470/abstract

Keating, S.T., Groh, L., van der Heijden, C.D.C.C., Rodriguez, H., Santos, dos, J.C., Fanucchi, S., Okabe, J., Kaipananickal, H., van Puffelen, J.H., Helder, L., Noz, M.P., Matzaraki, V., Li, Y., de Bree, L.C.J., Koeken, V.A.C.M., Moorlag, S.J.C.F.M., Mourits, V.P., Domínguez-Andrés, J., Oosting, M., Bulthuis, E.P., Koopman, W.J.H., Mhlanga, M., El-Osta, A., Joosten, L.A.B., Netea, M.G., Riksen, N.P., 2020. The Set7 Lysine Methyltransferase Regulates Plasticity in Oxidative Phosphorylation Necessary for Trained Immunity Induced by β-Glucan. CellReports 31, 107548. doi:10.1016/j.celrep.2020.107548

Krishack, P.A., Louviere, T.J., Decker, T.S., Kuzel, T.G., Greenberg, J.A., Camacho, D.F., Hrusch, C.L., Sperling, A.I., Verhoef, P.A., 2019. Protection against Staphylococcus aureus bacteremia-induced mortality depends on ILC2s and eosinophils. JCI Insight 4. doi:10.1172/jci.insight.124168

Lebman, D.A., Coffman, R.L., 1988. Interleukin 4 causes isotype switching to IgE in T cell-stimulated clonal B cell cultures. J Exp Med 168, 853–862. doi:10.1084/jem.168.3.853

Liu, P.-S., Wang, H., Li, X., Chao, T., Teav, T., Christen, S., Di Conza, G., Cheng, W.-C., Chou, C.-H., Vavakova, M., Muret, C., Debackere, K., Mazzone, M., Huang, H.-D., Fendt, S.-M., Ivanišević, J., Ho, P.-C., 2017. α-ketoglutarate orchestrates macrophage activation through metabolic and epigenetic reprogramming. Nature Immunology 18, 985–994. doi:10.1038/ni.3796

Locati, M., Curtale, G., Mantovani, A., 2020. Diversity, Mechanisms, and Significance of Macrophage Plasticity. Annu Rev Pathol 15, 123–147. doi:10.1146/annurev-pathmechdis-012418-012718

Major, J., Fletcher, J.E., Hamilton, T.A., 2002. IL-4 pretreatment selectively enhances cytokine and chemokine production in lipopolysaccharide-stimulated mouse peritoneal macrophages. J Immunol 168, 2456–2463. doi:10.4049/jimmunol.168.5.2456

Orecchioni, M., Ghosheh, Y., Pramod, A.B., Ley, K., 2019. Macrophage Polarization: Different Gene Signatures in M1(LPS+) vs. Classically and M2(LPS-) vs. Alternatively Activated Macrophages. Front Immunol 10, 1084. doi:10.3389/fimmu.2019.01084

Peters, U., Dixon, A.E., Forno, E., 2018. Obesity and asthma. Journal of Allergy and Clinical Immunology 141, 1169–1179.

Sarfati, M., Fournier, S., Christoffersen, M., Biron, G., 1990. Expression of CD23 antigen and its regulation by IL-4 in chronic lymphocytic leukemia. Leukemia Research 14, 47–55. doi:https://doi.org/10.1016/0145-2126(90)90145-Y

Satoh, T., Takeuchi, O., Vandenbon, A., Yasuda, K., Tanaka, Y., Kumagai, Y., Miyake, T., Matsushita, K., Okazaki, T., Saitoh, T., Honma, K., Matsuyama, T., Yui, K., Tsujimura, T., Standley, D.M., Nakanishi, K., Nakai, K., Akira, S., 2010. The Jmjd3-Irf4 axis regulates M2

macrophage polarization and host responses against helminth infection. Nature Immunology 11, 936–944. doi:10.1038/ni.1920

Sica, A., Mantovani, A., 2012. Macrophage plasticity and polarization: in vivo veritas. J Clin Invest 122, 787–795. doi:10.1172/JCI59643

Snoeck, H.W., Lardon, F., van Bockstaele, D.R., Peetermans, M.E., 1993. Effects of interleukin-4 (IL4) on myelopoiesis: studies on highly purified CD34+ hematopoietic progenitor cells. Leukemia 7, 625–629. doi:10.1007/BF01700376

Sonoda, Y., 1994. Interleukin-4--a dual regulatory factor in hematopoiesis. Leuk Lymphoma 14, 231–240. doi:10.3109/10428199409049673

Stuart, P.M., Zlotnik, A., Woodward, J.G., 1988. Induction of class I and class II MHC antigen expression on murine bone marrow-derived macrophages by IL-4 (B cell stimulatory factor 1). J Immunol 140, 1542–1547.

Sutherland, R.E., Xu, X., Kim, S.S., Seeley, E.J., Caughey, G.H., Wolters, P.J., 2011. Parasitic infection improves survival from septic peritonitis by enhancing mast cell responses to bacteria in mice. PLoS One 6, e27564. doi:10.1371/journal.pone.0027564

Tannahill, G.M., Curtis, A.M., Adamik, J., Palsson-McDermott, E.M., McGettrick, A.F., Goel, G., Frezza, C., Bernard, N.J., Kelly, B., Foley, N.H., Zheng, L., Gardet, A., Tong, Z., Jany, S.S., Corr, S.C., Haneklaus, M., Caffrey, B.E., Pierce, K., Walmsley, S., Beasley, F.C., Cummins, E., Nizet, V., Whyte, M., Taylor, C.T., Lin, H., Masters, S.L., Gottlieb, E., Kelly, V.P., Clish, C., Auron, P.E., Xavier, R.J., O'Neill, L.A.J., 2013. Succinate is an inflammatory signal that induces IL-1β through HIF-1α. Nature 496, 238–242. doi:10.1038/nature11986

Varin, A., Mukhopadhyay, S., Herbein, G., Gordon, S., 2010. Alternative activation of macrophages by IL-4 impairs phagocytosis of pathogens but potentiates microbial-induced signalling and cytokine secretion. Blood 115, 353–362. doi:10.1182/blood-2009-08-236711

Viola, A., Munari, F., Sánchez-Rodríguez, R., Scolaro, T., Castegna, A., 2019. The Metabolic Signature of Macrophage Responses. Front Immunol 10, 1462. doi:10.3389/fimmu.2019.01462

Wilson, J.L., Nägele, T., Linke, M., Demel, F., Fritsch, S.D., Mayr, H.K., Cai, Z., Katholnig, K., Sun, X., Fragner, L., Miller, A., Haschemi, A., Popa, A., Bergthaler, A., Hengstschläger, M., Weichhart, T., Weckwerth, W., 2020. Inverse Data-Driven Modeling and Multiomics Analysis Reveals Phgdh as a Metabolic Checkpoint of Macrophage Polarization and Proliferation. CellReports 30, 1542–1552.e7. doi:10.1016/j.celrep.2020.01.011

Woytschak, J., Keller, N., Krieg, C., Impellizzieri, D., Thompson, R.W., Wynn, T.A., Zinkernagel, A.S., Boyman, O., 2016. Type 2 Interleukin-4 Receptor Signaling in Neutrophils Antagonizes Their Expansion and Migration during Infection and Inflammation. Immunity 45, 172–184. doi:10.1016/j.immuni.2016.06.025

Zein, J.G., Love, T.E., Erzurum, S.C., 2017. Asthma Is Associated with a Lower Risk of Sepsis and Sepsis-related Mortality. Am J Respir Crit Care Med 196, 787–790. doi:10.1164/rccm.201608-1583LE

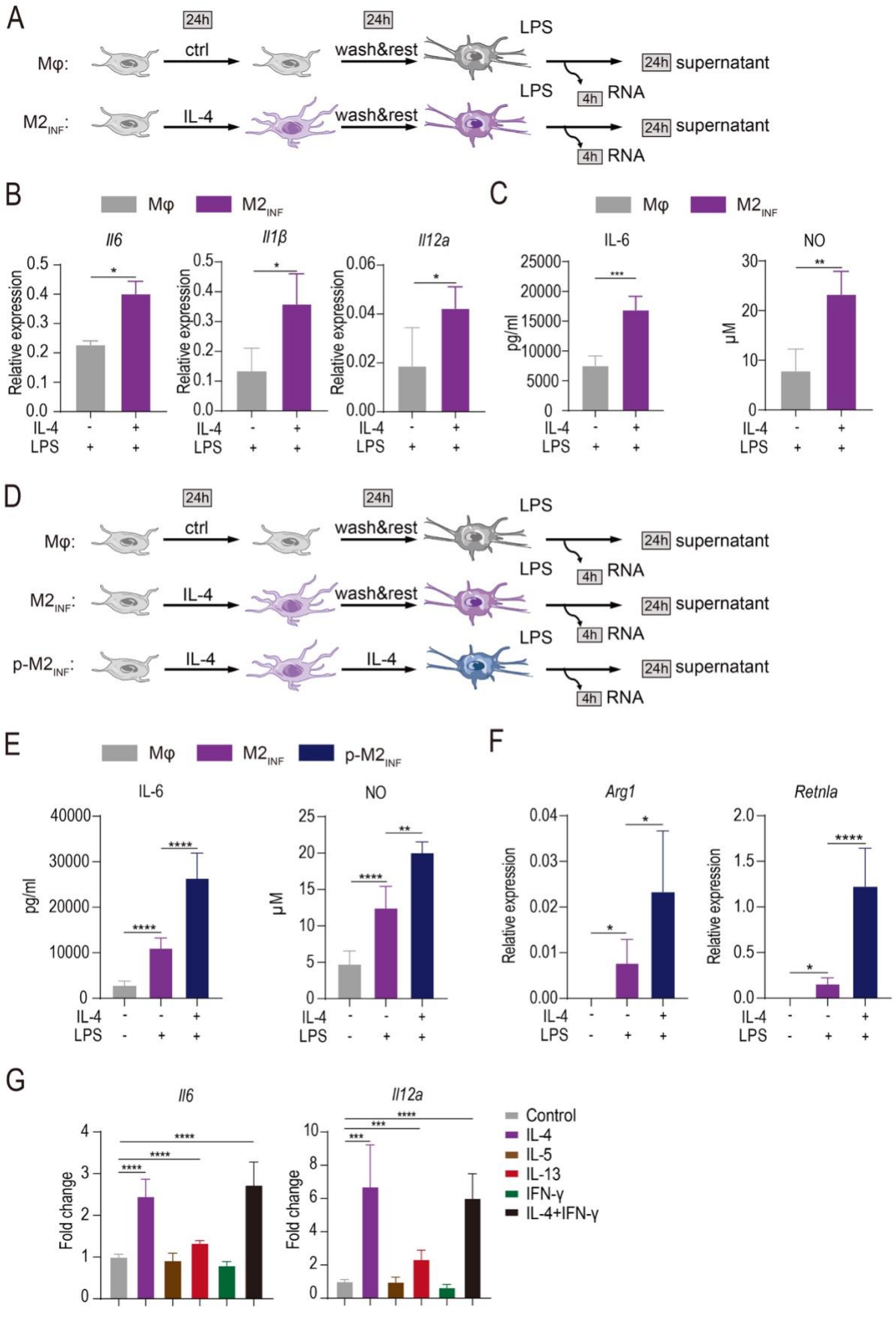
A
24h
ctrl
24h
wash&rest
LPS
Mφ:
24h supernatant
4h RNA
LPS
M2INF:
IL-4
wash&rest
24h supernatant
4h RNA
B
Mφ
M2INF
Il6
Il1β
Il12a
Relative expression
IL-4
LPS
C
Mφ
M2INF
IL-6
pg/ml
NO
μM
D
24h
ctrl
24h
wash&rest
LPS
Mφ:
24h supernatant
4h RNA
M2INF:
IL-4
wash&rest
p-M2INF:
IL-4
IL-4
E
Mφ
M2INF
p-M2INF
IL-6
pg/ml
NO
μM
F
Arg1
Retnla
Relative expression
G
Il6
Il12a
Fold change
Control
IL-4
IL-5
IL-13
IFN-γ
IL-4+IFN-γ

Figure 1. IL-4 induced non-canonical $M2_{INF}$. (**A**) Schematic presentation of the experimental setup for assessing IL-4 non-canonical effect on macrophages. (**B**) IL-4 stimulated BMDMs were stimulated with LPS for 4 hours, and mRNA was harvested for subsequent qPCR analysis. (**C**) IL-6 and NO production were determined from the culture supernatant 24 hours post LPS stimulation. **(D)** Experimental setup for assessing prolonged IL-4 stimulation effect. **(E)** IL-6 and NO production and **(F)** M2 gene expression were determined accordingly. **(G)** BMDMs pretreated with indicated cytokines were stimulated with LPS for 4 hours, and mRNA was harvested for subsequent qPCR analysis. *$P < 0.05$, unpaired, two-tailed Student's t-test. Data are representative of 3 independent experiments with 3 to 4 samples per group (mean ± SD).

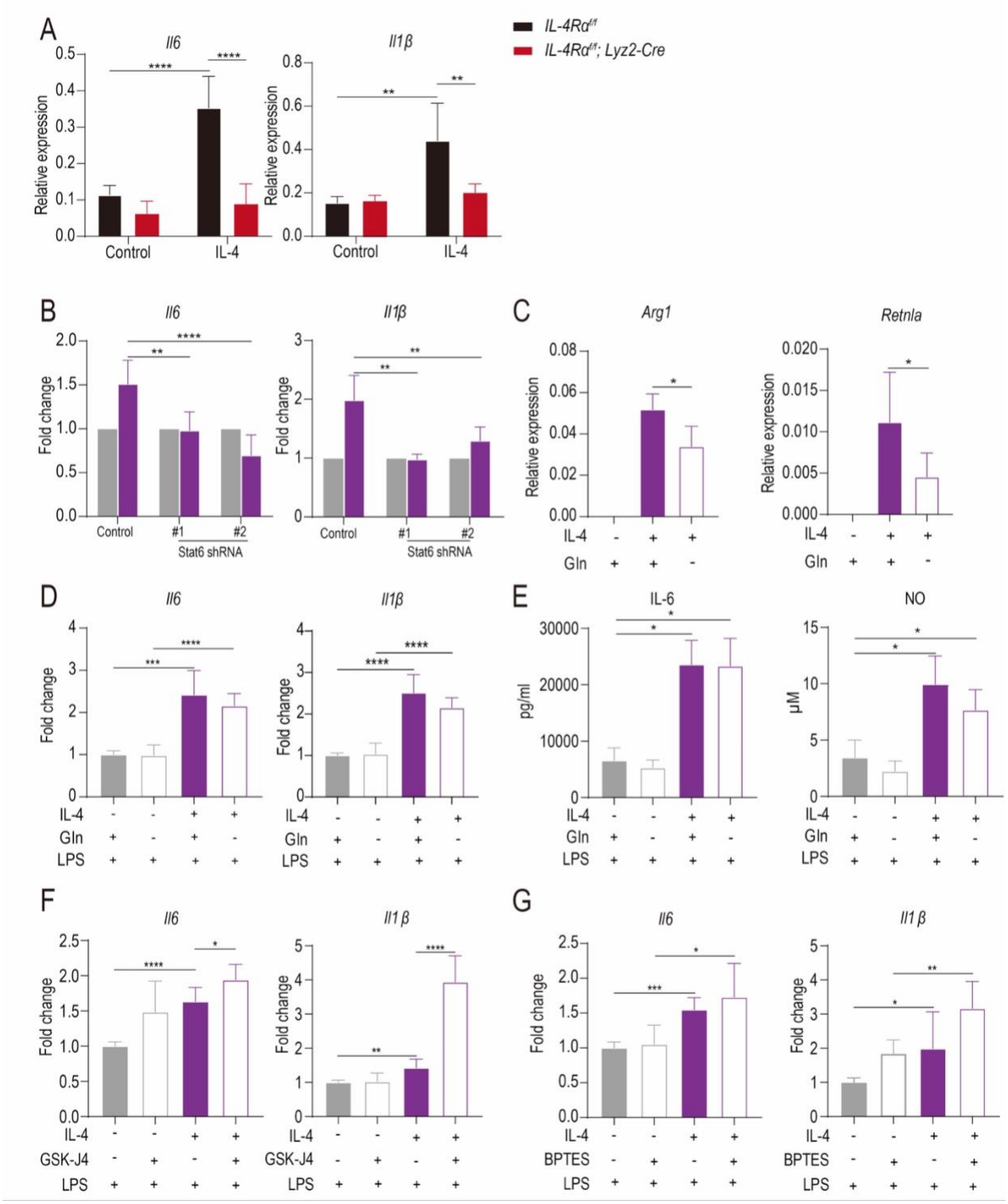

Figure 2. IL-4 induced M2$_{INF}$ in a Stat6-dependent and Gln/α-KG/Jmjd3 axis-independent manner. (A) qPCR mRNA expression of cytokine genes in Wildtype littermate and IL-4Rα MKO BMDMs stimulated with LPS at 24 hours post-IL-4 stimulation. qPCR mRNA expression of cytokine genes **(B, D, F&G)** and M2 marker genes **(C)** in BMDMs stimulated with IL-4 **(B)**, or LPS (**D, F&G**) at 24 hours post-IL-4 stimulation under various culture condition as indicated. **(E)** Corresponding IL-6 and NO production were measured from supernatant harvested 24 hours

post LPS stimulation. *P < 0.05, unpaired, two-tailed Student's t-test. Data are representative of 3 independent experiments with 3 to 4 samples per group (mean ± SD).

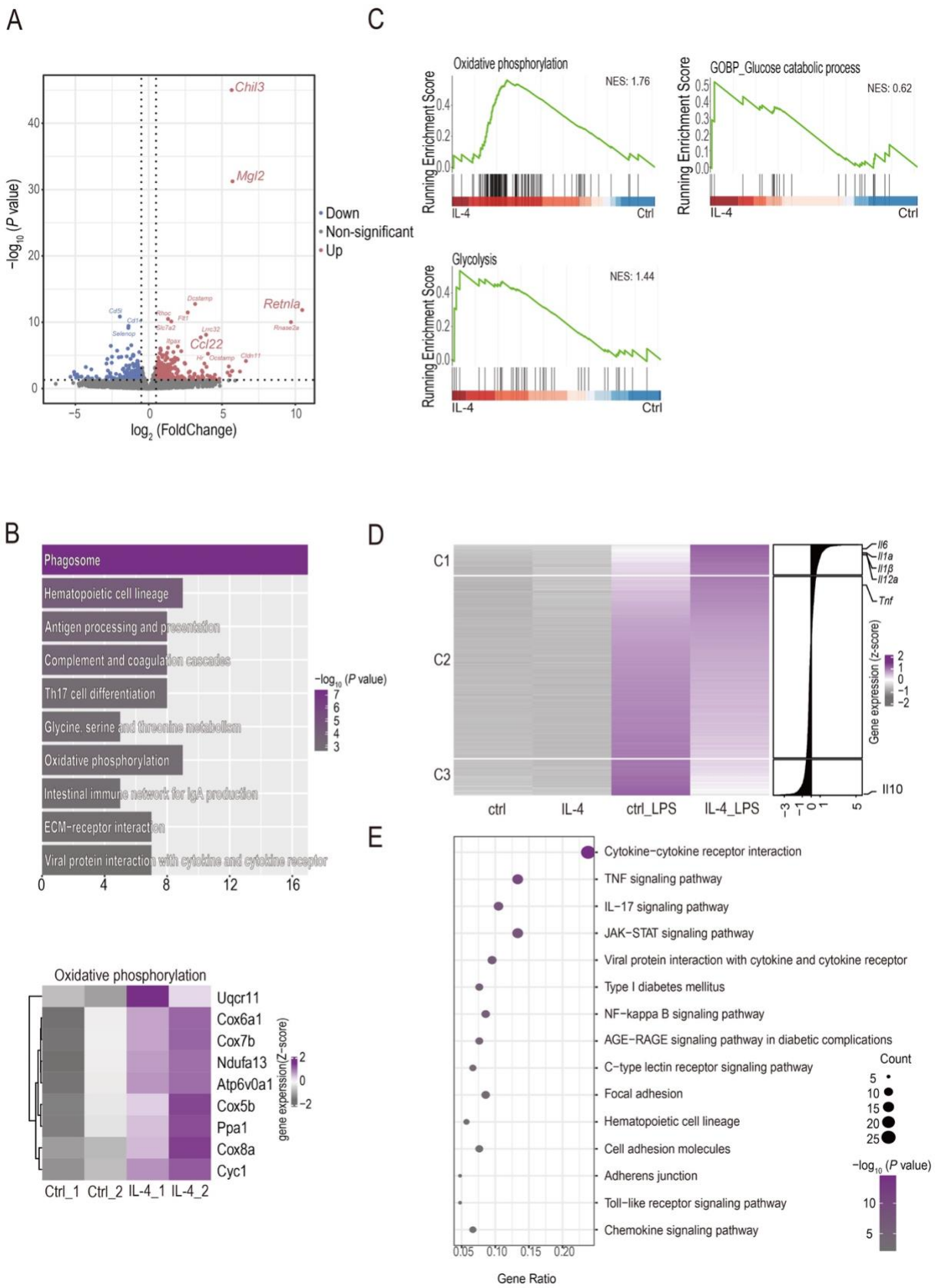
A
Chil3
Mgl2
Retnla
Ccl22
Down
Non-significant
Up
−log10 (P value)
log2 (FoldChange)
C
Oxidative phosphorylation
NES: 1.76
GOBP_Glucose catabolic process
NES: 0.62
Glycolysis
NES: 1.44
Running Enrichment Score
IL-4
Ctrl
B
Phagosome
Hematopoietic cell lineage
Antigen processing and presentation
Complement and coagulation cascades
Th17 cell differentiation
Glycine, serine and threonine metabolism
Oxidative phosphorylation
Intestinal immune network for IgA production
ECM−receptor interaction
Viral protein interaction with cytokine and cytokine receptor
−log10 (P value)
Oxidative phosphorylation
Uqcr11
Cox6a1
Cox7b
Ndufa13
Atp6v0a1
Cox5b
Ppa1
Cox8a
Cyc1
gene expression(Z-score)
Ctrl_1 Ctrl_2 IL-4_1 IL-4_2
D
C1
C2
C3
ctrl
IL-4
ctrl_LPS
IL-4_LPS
Il6
Il1a
Il1β
Il12a
Tnf
Il10
Gene expression (z-score)
E
Cytokine−cytokine receptor interaction
TNF signaling pathway
IL−17 signaling pathway
JAK−STAT signaling pathway
Viral protein interaction with cytokine and cytokine receptor
Type I diabetes mellitus
NF−kappa B signaling pathway
AGE−RAGE signaling pathway in diabetic complications
C−type lectin receptor signaling pathway
Focal adhesion
Hematopoietic cell lineage
Cell adhesion molecules
Adherens junction
Toll−like receptor signaling pathway
Chemokine signaling pathway
Count
−log10 (P value)
Gene Ratio

730

Figure 3. The transcriptomic profile of $M2_{INF}$. (**A**) The volcano plot of the differential expressed genes between control and IL-4-treated BMDMs. **(B)** Top 10 pathways enriched by KEGG analysis of the IL-4 upregulated genes. **(C)** Enrichment of oxidative phosphorylation, glucose catabolic process, and glycolysis in IL-4 treated macrophage in GSEA. **(D)** Control and IL-4-treated BMDMs were stimulated with LPS or left untreated for 4 hours. LPS upregulated genes were filtered out, and the expression level was ranked normalized according to the Log2FC value between the control-LPS group and IL-4-LPS group. Genes were further divided into three clusters: C1 (Log2FC ≥0.5), C2 (0.5 ≥ Log2Fc ≥ -0.5), and C3 (Log2FC ≤ -0.5). **(E)** GO analysis of the genes in the C1 cluster.

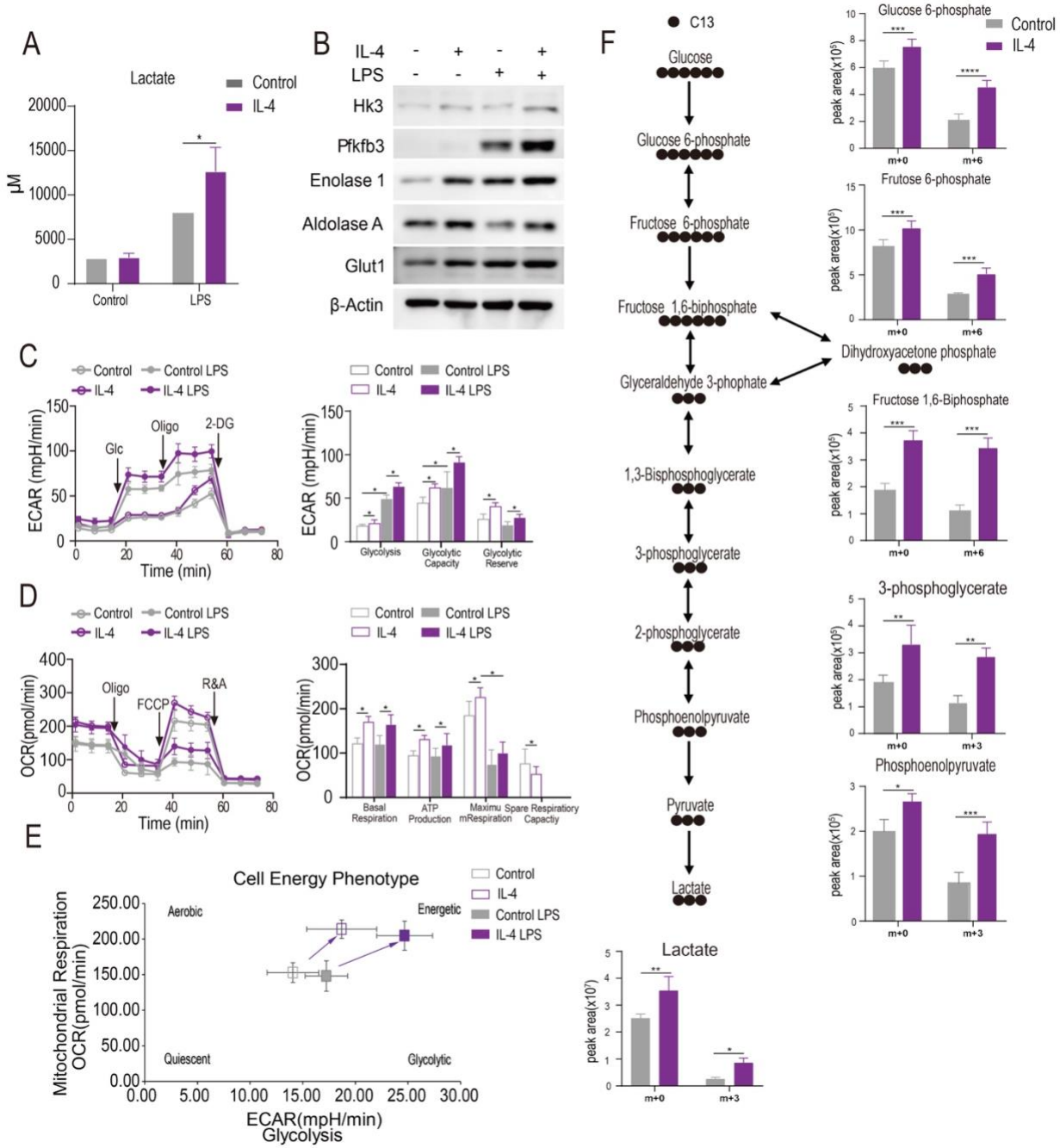

Figure 4. Metabolic characterization of $M2_{INF}$. (**A**) Concentration of lactate in the supernatants harvested from $M2_{INF}$ stimulated with LPS for 24 hours. (**B**) Western blot of Hk3, Pfkfb3, Enolase1, Aldolase A, Glut1 and β-actin in control or $M2_{INF}$ stimulated with LPS for 3 hours Representative blots of three independent experiments are shown. Seahorse analysis of control or $M2_{INF}$ at basal or 3 hours post LPS stimulation. ECAR and glycolysis capacity (**C**) and OCR and mitochondrial respiration capacity (**D**) were determined from two independent experiments. **(E)** Cell energetic profiles of BMDMs from control and $M2_{INF}$ at both basal and LPS stimulated states were depicted. **(F)** Representative metabolites derived from $^{13}C_6$-Glucose following the glycolysis pathway determined by LC-MS/MS were shown.

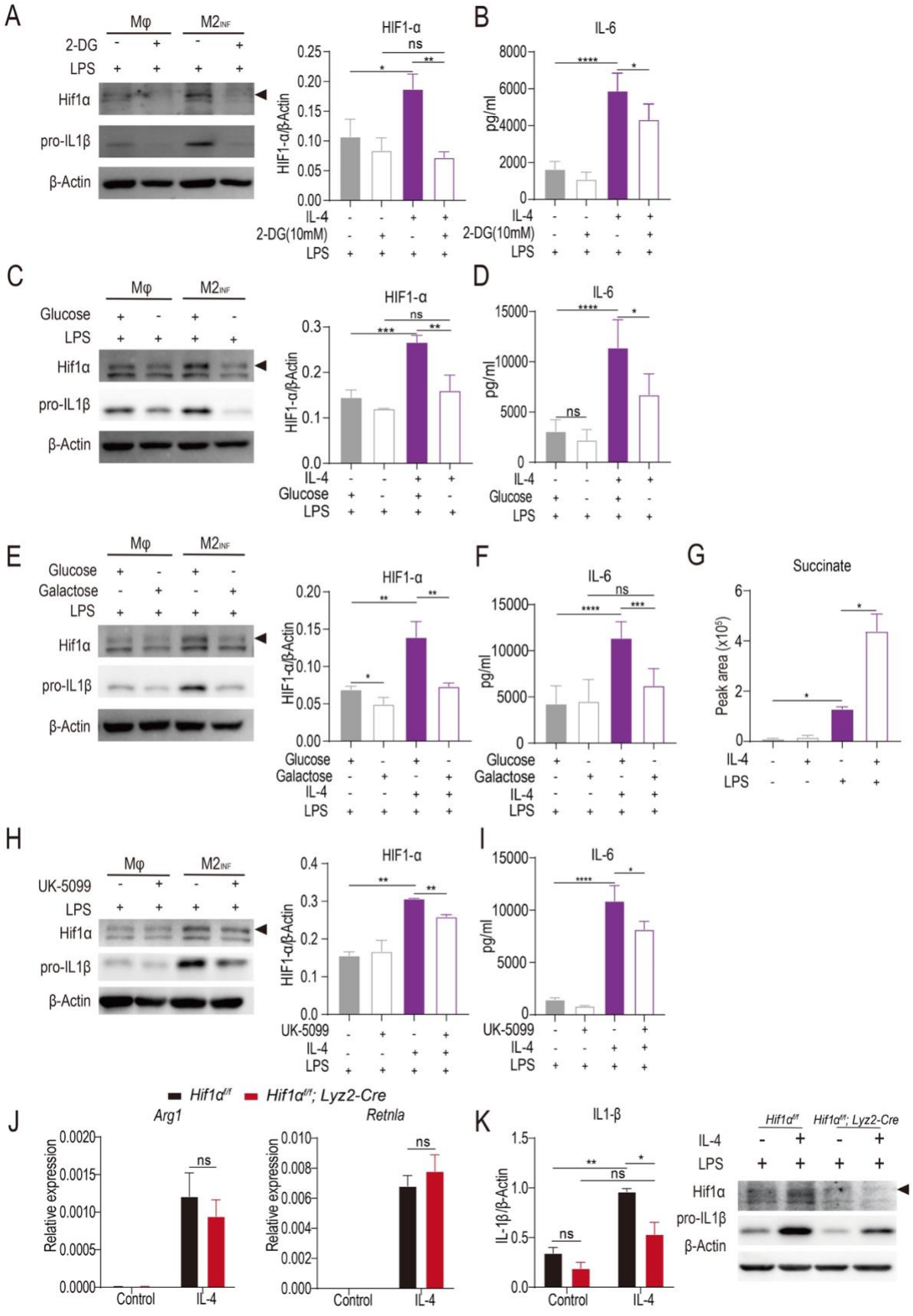
A
Mφ
M2INF
2-DG
LPS
Hif1α
pro-IL1β
β-Actin
HIF1-α
HIF1-α/β-Actin
IL-4
2-DG(10mM)
LPS
B
IL-6
pg/ml
C
Glucose
D
E
Galactose
F
G
Succinate
Peak area (x10⁵)
H
UK-5099
I
J
Hif1α^f/f
Hif1α^f/f; Lyz2-Cre
Arg1
Retnla
Relative expression
Control
K
IL1-β
IL-1β/β-Actin

751

Figure 5. Glycolysis/Hif-1α axis is critical for $M2_{INF}$. Control or $M2_{INF}$ macrophages were stimulated with LPS in the presence or absence of **(A-B)** 2-DG, **(C-D)** glucose, **(E-F)** galactose or **(H-I)** UK5099. Cell lysate were harvested for western blot analysis. Hif-1α and pro-IL-1β level and *Il6* expression were determined by western blot and qPCR, respectively. **(G)** Succinate level from control and $M2_{INF}$ macrophages were determined by LC-MS. **(J)** Wildtype littermate and Hif-1α MKO BMDMs were treated with IL-4 for 24 hours. mRNA was harvested for *Arg1* and *Rentla* expression determined by qPCR. **(K)** Control or $M2_{INF}$ macrophages from wild type or Hif-1α MKO were stimulated with LPS. Hif-1α and pro-IL-1β and β-actin levels were determined by Western blot analysis.

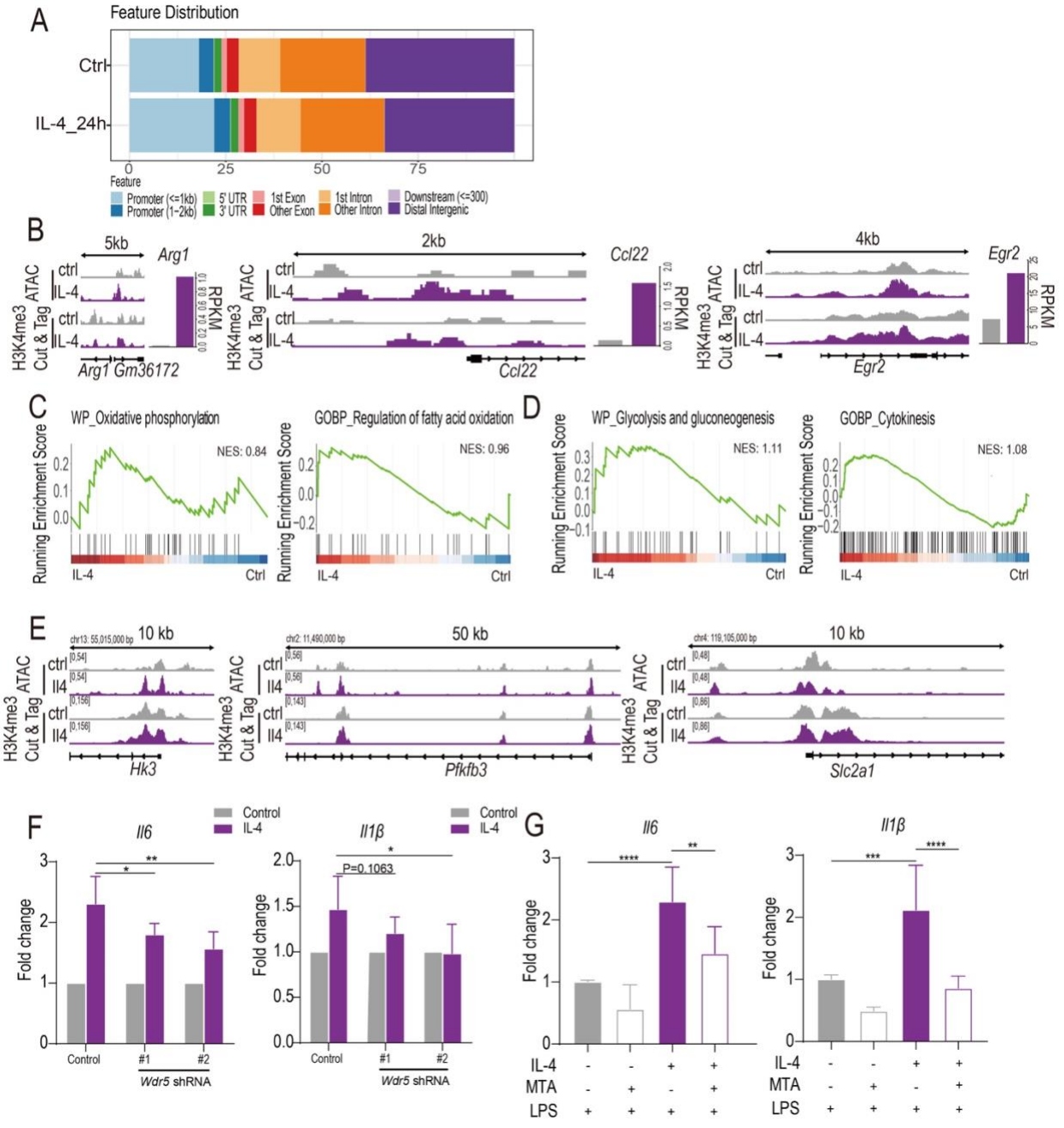

Figure 6. Epigenetic profiles of M2INF. **(A)** Distributions of differential ATAC-seq peaks incontrol and IL-4-treated BMDMs. **(B)** Representative ATACseq screenshots M2 marker genes, such as *Ccl22*, *Arg1* and *Egr2* of control or IL-4-treated BMDMs. RPKM of corresponding gene was depicted in bar-plot. GSEA enrichment of **(C)** oxidative phosphorylation, fatty acid oxidation and **(D)** glycolysis and cytokine pathways in IL-4 treated macrophage. **(E)** Representative ATACseq and H3K4me3 Cut&Tag screenshots of glycolysis genes in control or IL-4-stimulated BMDMs. **(F)** Control or *Wdr5* stable knockdown Raw264.7 cells were pretreated with IL-4 for 24 hours and stimulated with LPS for 4 hours to assess the mRNA expression of *Il6* and *Il1β* by qPCR. **(G)** qPCR mRNA expression of cytokine genes in BMDMs pre-treated with MTA for 30 minutes followed by 24 hours IL-4 stimulation. The gene expression was determined 4 hours post LPS

773 stimulation. *P < 0.05, unpaired, two-tailed Student's t-test. Data are representative of 3
774 independent experiments with 3 samples per group (mean ± SD).

775

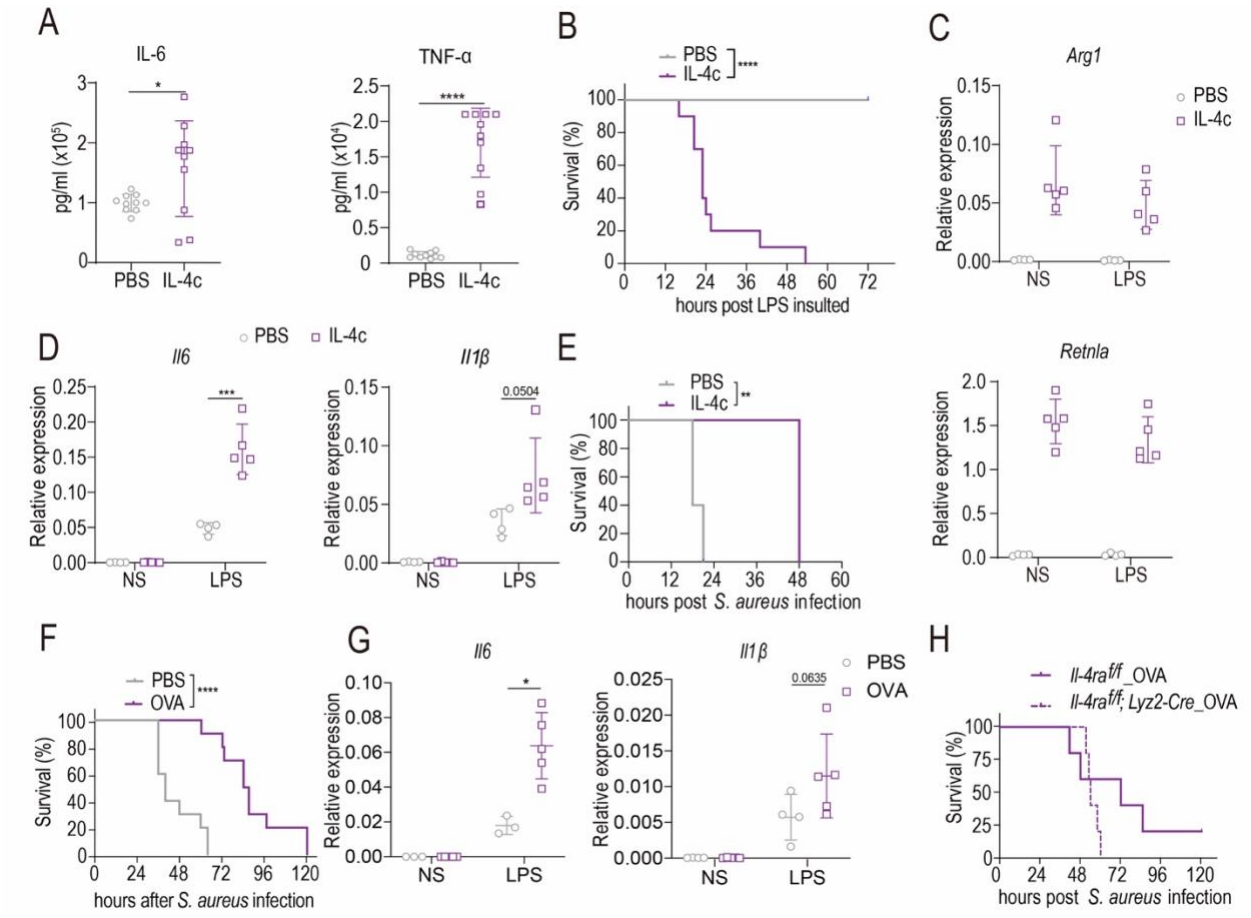

Figure 7. IL-4 induced M2$_{INF}$ *in vivo*. (**A**) IL-6 and TNF-α were determined from serum taken 3 hours post LPS injection in control and IL-4c treated mice. Survival of wild-type C57BL/6J pretreated with PBS or IL-4c for 24 hours followed by (B) LPS i.p. injection or (**E**) *S. aureus* infection. Data are representative of 2 independent experiments with 10 mice per group. (**C**) qPCR analysis of the M2 marker genes from peritoneal macrophages isolated from IL-4c-treated or PBS control group. (**D**) Peritoneal macrophages from the IL-4c-treated or PBS control group were stimulated with LPS for 4 hours *ex vivo*. The expression of cytokine genes was determined by qPCR. **(F&H)** Wild type Mice **(F)** and Wildtype littermate and *Il-4ra* MKO mice **(H)** were primed with OVA-Alum twice at Day1 and Day 14. From day 21 to 25, mice were given OVA via i.p. daily. 6 hours post last OVA challenge, mice were infected with *S. aureus* and survival was monitored. **(G)** Peritoneal macrophages from the OVA challenged or PBS control group were stimulated with LPS for 4 hours *ex vivo*. The expression of cytokine genes was determined by qPCR. *P < 0.05, unpaired, two-tailed Student's t-test. Data are representative of 2 independent experiments with 10 mice per group (mean ± SD).

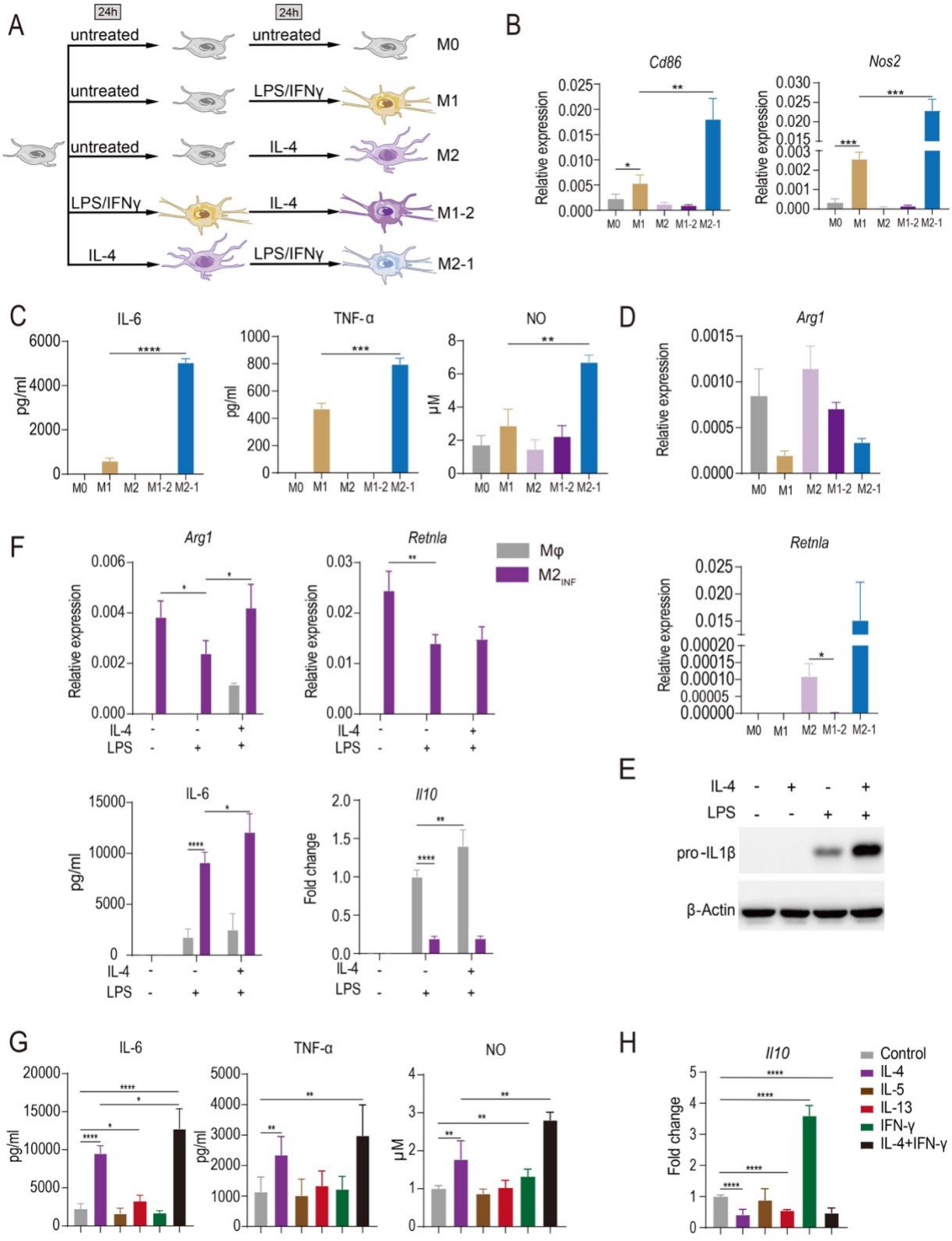

Supplementary Figure 1. **(A)** Schematic presentation of the experimental setup for macrophages polarization and repolarization. **(B)** BMDMs were polarized with IFN-γ and LPS (M1), IL-4 (M2) for 24 hours, or subsequently repolarized with opposed cytokines for additional

24 hours. The expression of *Cd86* and *Nos2* was determined by qPCR. **(C)** The IL-6, TNF-α, and NO level in the culture supernatant were determined by ELISA and Griess assay, respectively. **(D)** M2 marker gene expression during macrophage polarization and repolarization. **(E)** Control or IL-4-treated macrophages were stimulated with LPS for 3 hours. Cell lysate were harvested for pro-IL-1β western blot analysis. **(F)** Control or $M2_{IFN}$ were stimulated with LPS in the presence of absence of IL-4. M2 and cytokine gene expression were determined by qPCR. **(G)** Different cytokine stimulated BMDMs were stimulated with LPS for 24 hours, and supernatant was harvested for IL-6 and NO determination. **(H)** Different cytokine stimulated BMDMs were stimulated with LPS for 4 hours, and *Il10* mRNA expression was determined by qPCR. *P < 0.05, unpaired, two-tailed Student's t-test. Data are representative of 2 independent experiments with 10 mice per group (mean ± SD).

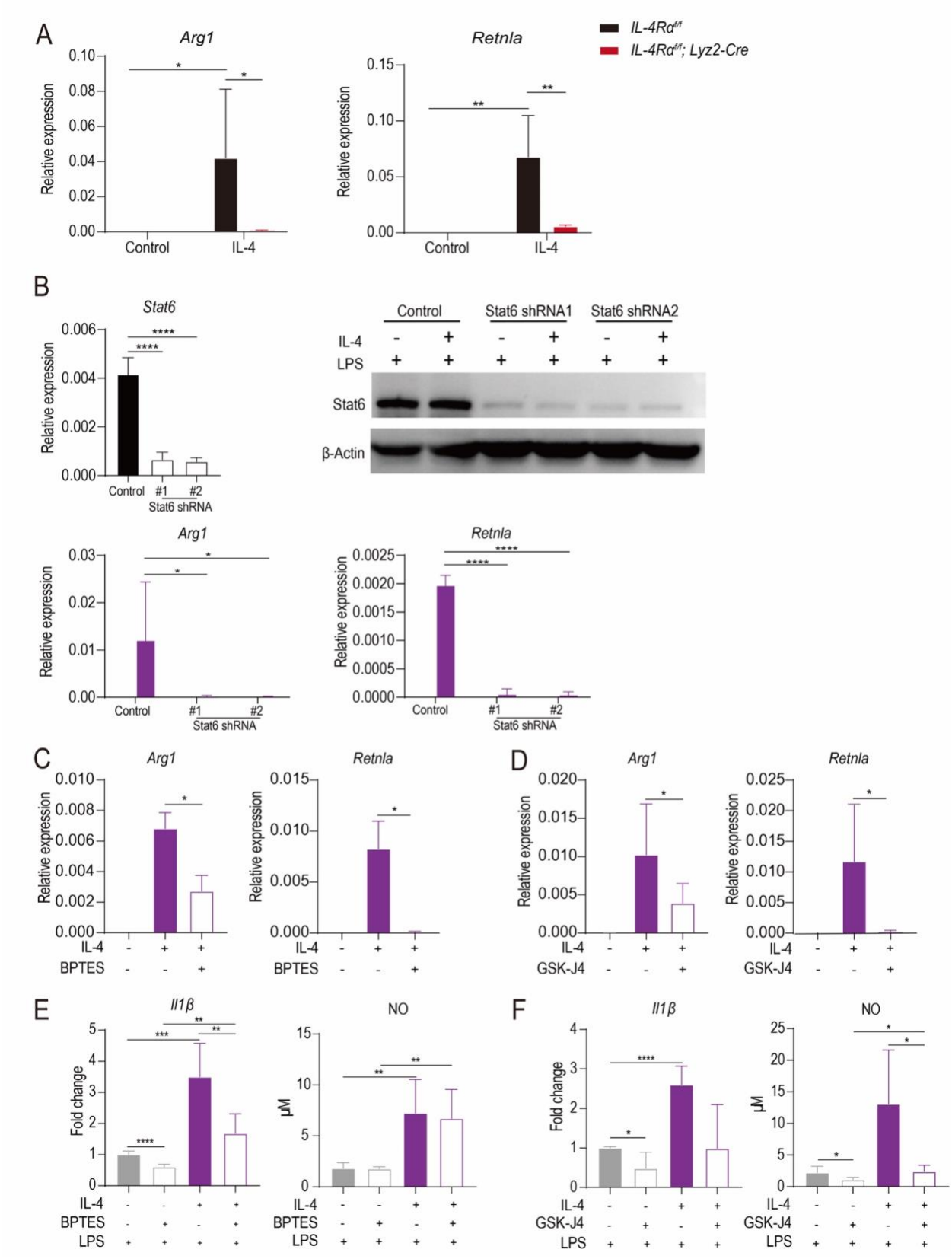

Supplementary Figure 2. (A) qPCR mRNA expression of M2 marker genes in Wildtype littermate and IL-4Rα MKO BMDMs at 24 hours post-IL-4 stimulation. **(B)** Stat6 knock down

efficiency was determined by qPCR and western blot. qPCR mRNA expression of M2 marker genes **(C&D)**, cytokine genes **(E&F)** in BMDMs stimulated with IL-4 **(C&D)**, or LPS **(E&F)** at 24 hours post-IL-4 stimulation under various culture condition as indicated. *P < 0.05, unpaired, two-tailed Student's t-test. Data are representative of 3 independent experiments with 3 to 4 samples per group (mean ± SD).

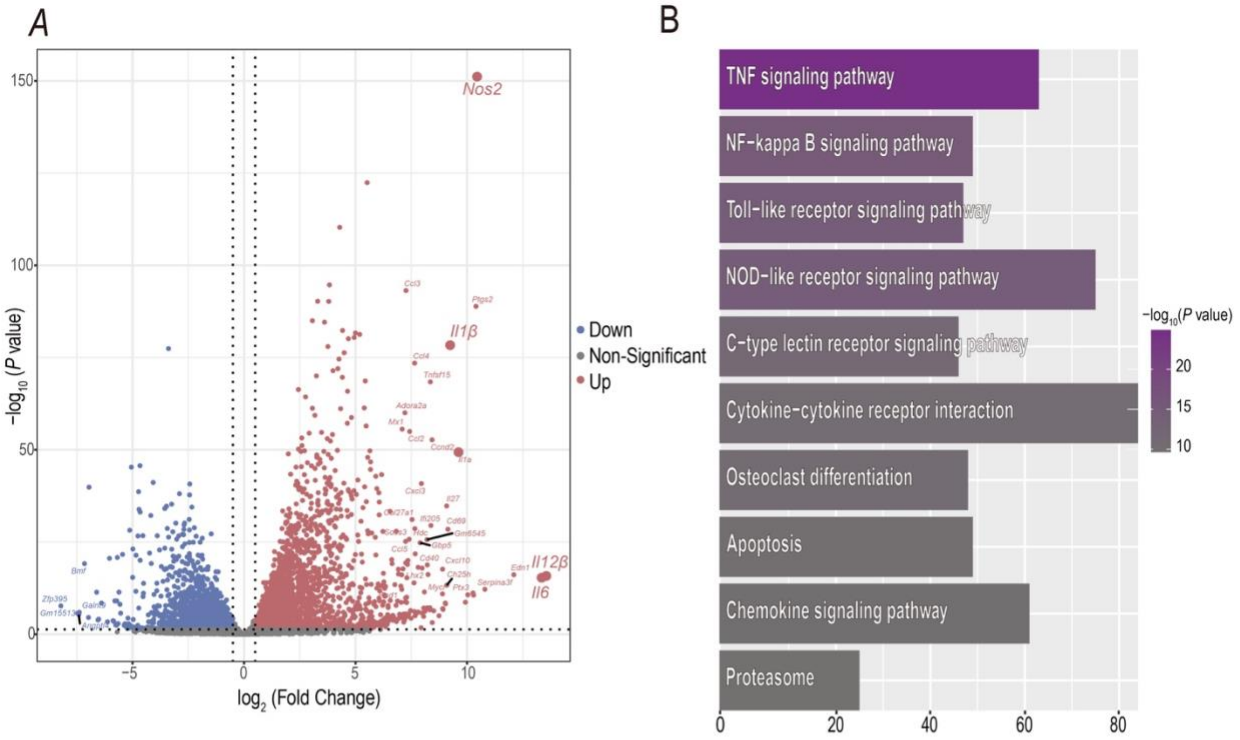

C

	Description	*P* value
Cluster I	Cytokine-cytokine receptor interaction	2.56E-15
	TNF signaling pathway	4.29E-11
	IL-17 signaling pathway	7.71E-09
	JAK-STAT signaling pathway	8.62E-09
	Viral protein interaction with cytokine and cytokine receptor	1.47E-07
	Type I diabetes mellitus	1.46E-06
	NF-kappa B signaling pathway	3.64E-06
	AGE-RAGE signaling pathway in diabetic complications	2.32E-05
	C-type lectin receptor signaling pathway	3.39E-04
	Focal adhesion	5.85E-04
Cluster II	TNF signaling pathway	5.13E-19
	NOD-like receptor signaling pathway	6.71E-14
	NF-kappa B signaling pathway	1.35E-10
	Toll-like receptor signaling pathway	1.86E-10
	Apoptosis	1.76E-09
	Cytosolic DNA-sensing pathway	3.81E-09
	Osteoclast differentiation	5.79E-09
	RIG-I-like receptor signaling pathway	3.17E-08
	C-type lectin receptor signaling pathway	6.22E-08
	Necroptosis	9.62E-07
Cluster III	Cytokine-cytokine receptor interaction	3.87E-10
	Viral protein interaction with cytokine and cytokine receptor	2.22E-05
	JAK-STAT signaling pathway	2.36E-04
	Hematopoietic cell lineage	1.09E-03
	Cell adhesion molecules	1.44E-03
	Toll-like receptor signaling pathway	1.50E-03
	Intestinal immune network for IgA production	1.94E-03
	Chemokine signaling pathway	2.67E-03
	Th1 and Th2 cell differentiation	4.73E-03
	Phagosome	7.54E-03

Supplementary Figure 3. **(A)** Enrichment of Mapk, Nf-κb, and Hif-1α pathway in IL-4 treated macrophage in GSEA. **(B)** The volcano plot of the differential expressed genes between control and LPS-treated BMDMs. **(C)** Top 10 pathways enriched by KEGG analysis of the LPS upregulated genes. **(D)** Top 10 pathways enriched by KEGG analysis of different clusters enriched in IL-4-LPS upregulated genes.

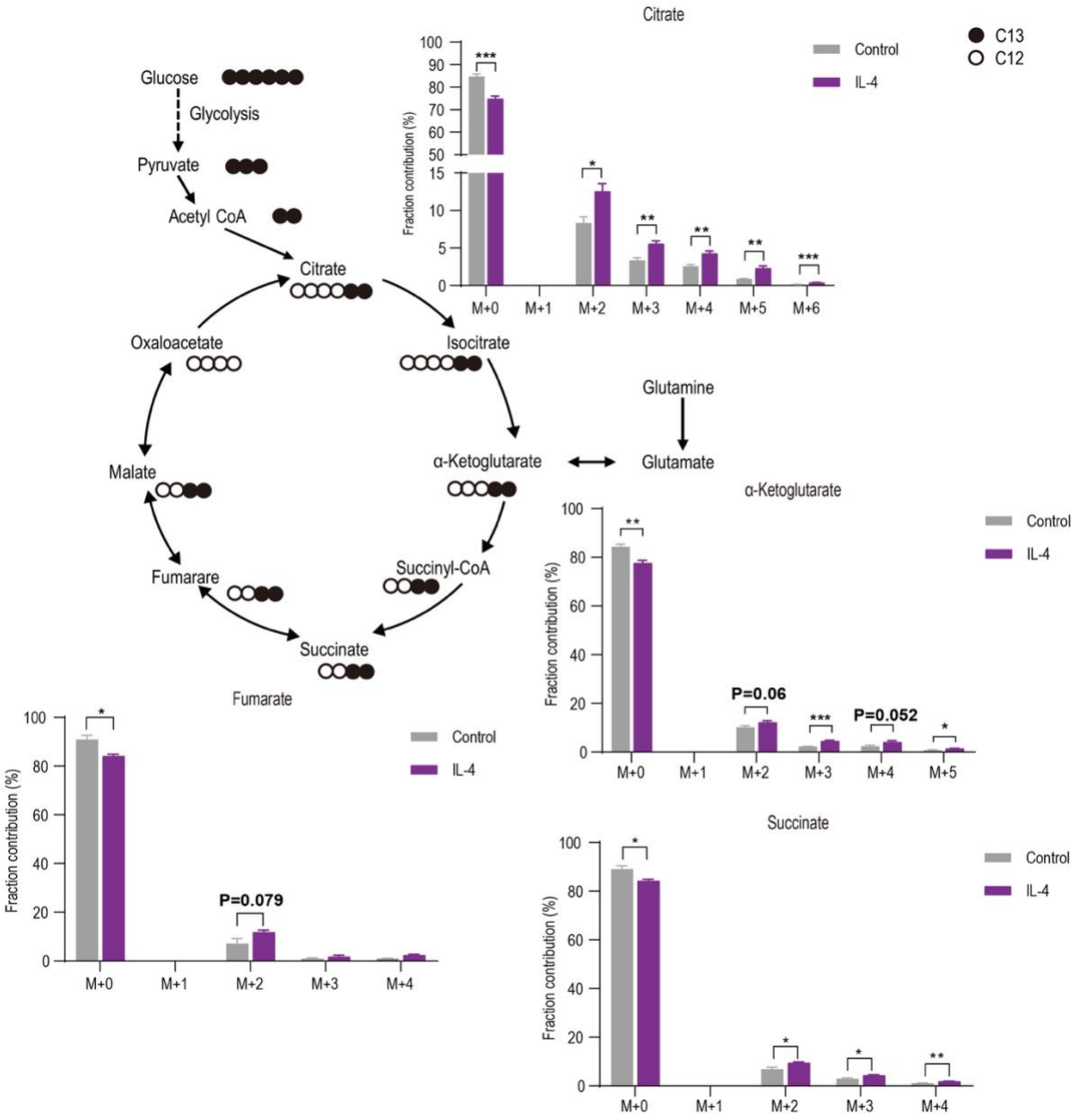
Glucose
Glycolysis
Pyruvate
Acetyl CoA
Citrate
Isocitrate
α-Ketoglutarate
Succinyl-CoA
Succinate
Fumarare
Malate
Oxaloacetate
Glutamine
Glutamate
C13
C12
Control
IL-4
Citrate
Fraction contribution (%)
M+0
M+1
M+2
M+3
M+4
M+5
M+6
α-Ketoglutarate
P=0.06
P=0.052
Fumarate
P=0.079
Succinate

826

Supplementary Figure 4. Representative metabolites derived from 13C6-Glucose following TCA cycle pathway determined by LC-MS/MS were shown.

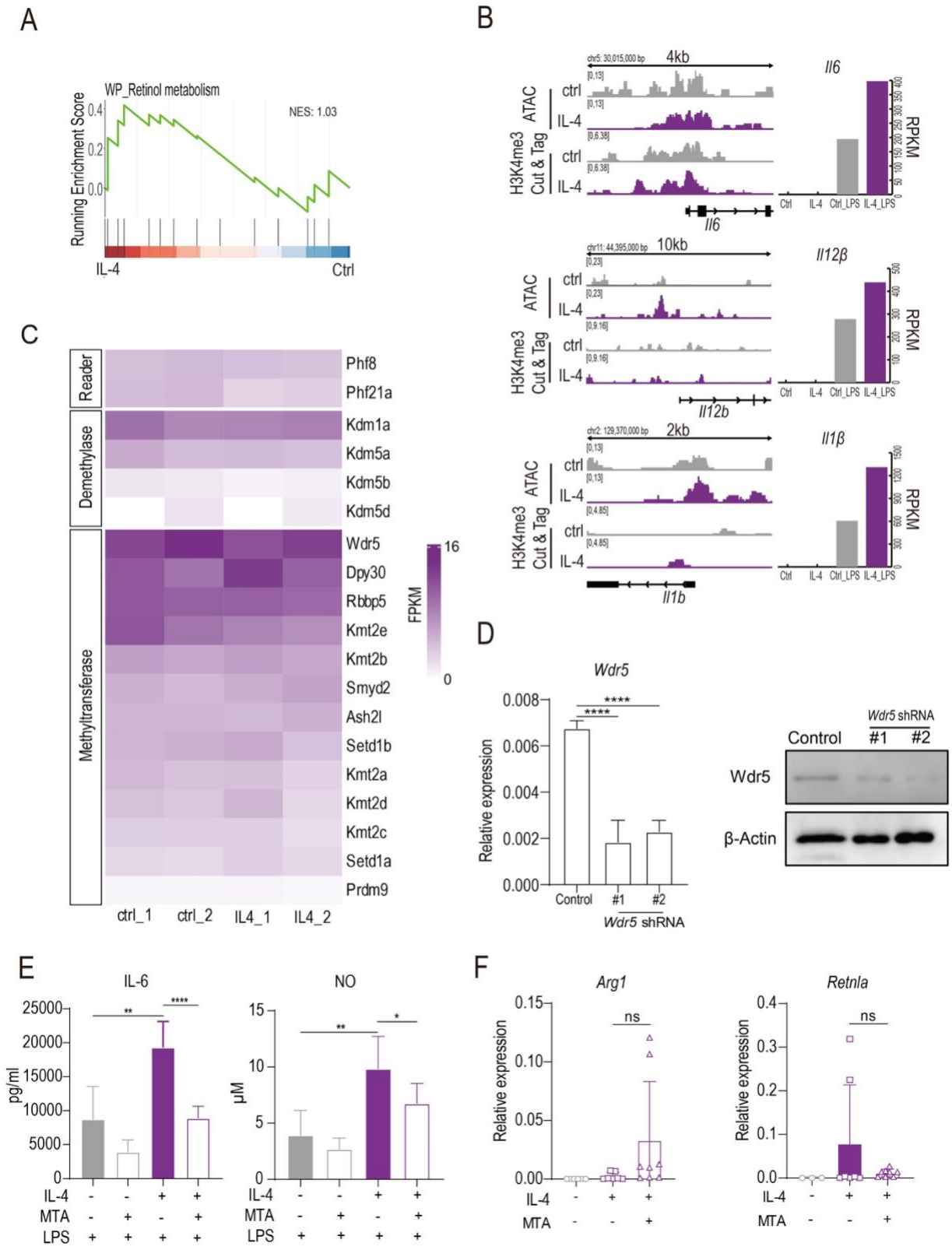

830

Supplementary Figure 5. **(A)** Retinol metabolism was enriched by GSEA analysis in IL-4 treated macrophages. **(B)** Representative ATACseq and H3K4me3 Cut&Tag screenshots of cytokine genes in control or IL-4-stimulated BMDMs. **(C)** 待补充 **(D)** Wdr5 knock down efficiency was determined by qPCR and western blot. **(E)** BMDMs were pretreated with MTA for 30 minutes and subsequently stimulated with IL-4 for 24 hours. BMDMs were stimulated with LPS for 24h and supernatant were harvested for ELISA. **(F)** Expression of *Arg1* and *Retnla* was determined by qPCR. *P < 0.05, unpaired, two-tailed Student's t-test. Data are representative of 2 independent experiments with 10 mice per group (mean ± SD).

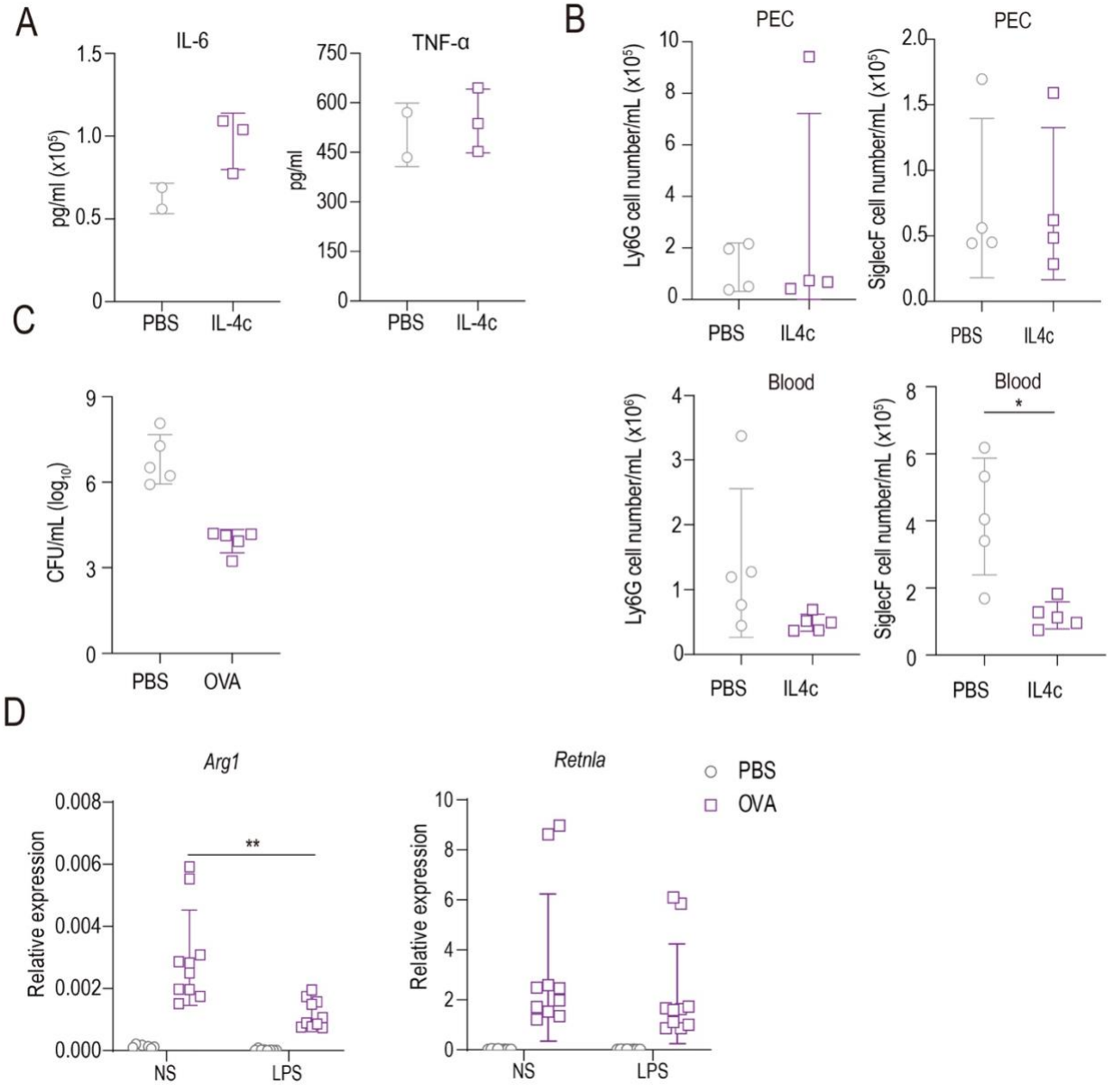

Supplementary Figure 6. **(A)** IL-6 and TNF-α were determined from peritoneal fluid taken 3 hours post LPS injection in control and IL-4c-treated mice. **(B)** Ly6C^{hi} and SiglecF expression in peritoneal cells and peripheral blood from control and IL-4c-treated mice. **(C)** Blood bacterial CFU determined from blood 3 h post-SA infection in control or OVA-allergy mice. **(D)** The M2 gene expression in peritoneal macrophages from the OVA challenged or PBS control group was determined by qPCR. *P < 0.05, unpaired, two-tailed Student's t-test. Data are representative of 2 independent experiments with 10 mice per group (mean ± SD).

Supplementary information

	Primer Sequences for RNA analysis
β2m F	TTCTGGTGCTTGTCTCACTGA
β2m R	CAGTATGTTCGGCTTCCCATTC
Chil3 F	CAGGTCTGGCAATTCTTCTG AA
Chil3 R	GTCTTGCTCATGTGTGTAAG TGA
Retnla F	TCCCAGTGAATACTGATGAGA
Retnla R	CCACTCTGGATCTCCCAAGA
Arg1 F	CCAGAAGAATGGAAGAGTCAGTGT
Arg1 R	GCAGATATGCAGGGAGTCACC
TNF-α F	CCCTCACACTCAGATCATCTTCT
TNF-α R	GCTACGACGTGGGCTACAG
IL-6 F	TAGTCCTTCCTACCCCAATTTCC
IL-6 R	TTGGTCCTTAGCCACTCCTTC
IL-10 F	GCTCTTACTGACTGGCATGA
IL-10 R	CGCAGCTCTAGGAGCATGTG
IL-12α F	CAATCACGCTACCTCCTCTTTT
IL-12αR	CAGCAGTGCAGGAATAATGTTTC
IL-1β F	TTCAGGCAGGCAGTATCACTC
IL-1β R	GAAGGTCCACGGGAAAGACAC
NOS2 F	GGAGTGACGGCAAACATGACT
NOS2 R	TCGATGCACAACTGGGTGAAC
CD86 F	CTGGACTCTACGACTTCACAATG
CD86 R	AGTTGGCGATCACTGACAGTT
Stat6 F	CTCTGTGGGGCCTAATTTCCA
Stat6 R	GCATCTGAACCGACCAGGAAC
Wdr5 F	CTCCTTGTGTCTGCCTCT GATG
Wdr5 R	CCTGAGACGATGAGGT TGGACT

Table S1. Sequences of primers used for quantitative real-time PCR. F and R refer to forward and reverse primers for quantitative real-time PCR.

	shRNA sequences used for stable gene knockdown
Wdr5-1	GCAGCGTTAGAGAACGACAAA
Wdr5-2	GCCGTTCATTTCAACCGTGAT
Stat6-1	AGCAGGAAGAACTCAAGTTTA
Stat6-2	CCGGGATCTTGCTCAGTTAAA

Table S2. Short hairpin RNA Sequences for constructing knock down plasmids target WDR5 and STAT6.